Supporting Information

Chirality-Induced Stereoselective Synthesis of Chiral sp^2-Carbon-Conjugated Covalent Organic Frameworks

Weijun Weng,[a] Zihan Zhu,[a] Xiaoyan Xu,[a] Jia Guo*[a]

[a]State Key Laboratory of Molecular Engineering of Polymers, Department of Macromolecular Science, Fudan University, Shanghai 200433, China.

*E-mail: guojia@fudan.edu.cn (J. G.)

Section I. Materials and Methods

1. Materials

Anhydrous dioxane, anhydrous 1,3,5-trimethylbenzene, anhydrous acetonitrile trifluoroacetic acid, terephthalaldehyde, 4,4'-biphenyldicarboxaldehyde, 2,4,6-trimethyl-1,3,5-triazine and sodium hydroxide were purchased from Aladdin Industrial Corporation. (R/S)-1-Phenethylamine was purchased from TCI Shanghai. (S)-(+)-3,3-dimethyl-2-butylamine was purchased from Sigma-Aldrich. Tetrahydrofuran and triethylamine were purchased from Shanghai Chemical Regents Company. All the chemicals were used without further purification.

2. Characterizations

Wide-angle X-ray scattering (WAXS) measurements were carried out at room temperature using the Xeuss SAXS/WAXS system (Xenocs A65, France) with Cu Kα radiation (λ = 0.154 nm). Fourier transform infrared (FT IR) spectra were tested on a Fourier transformation infrared spectrometer (Thermo Fischer Nicolet 6700, USA) with KBr pellets. N_2 adsorption-desorption isotherms were recorded at 77 K by a TriStar II 3020 volumetric adsorption analyzer (Micromeritics, USA). Before the test, samples were degassed at 90°C for 24 h. The pore-size distributions were calculated based on the Nonlocal Density Functional Theory (NLDFT). ^{1}H NMR and ^{13}C NMR spectra were collected on a 400 MHz spectrophotometer (Bruker AVANCE III HD, Switzerland) at 298.15 K. Transmission electron microscopy (TEM) images were obtained using a field emission transmission electron microscope (FEI Tecnai G2 F20 S-Twin, USA) operating at 200 kV accelerating voltage. Scanning electron microscopy (SEM) images were obtained using a field emission scanning electron microscope (Zeiss Gemini SEM500, Germany) operating at 3 kV accelerating voltage. Circular dichroism spectra were carried out at room temperature using a Chirascan (Applied Photophysics Ltd, UK) without smoothing. Circularly polarized luminescence spectra were measured by the

fluorescence spectrophotometer CPL-300 (JASCO, Japan) and the obtained spectra don't smooth. The excitation wavelength was set at 420 nm for TT-COF and 451 nm for TB-COF. All samples were the ethylene glycol dispersions of COF solids (100 mg/L). Nonpolarized photoluminescence spectra was tested using a spectrophotometer FLS1000 (Edinburgh Instruments, UK). The lifetimes were examined with a 450-nm diode laser using Time-Correlated Single Photon Counting (TCSPC) technique and calculated by fitting with first-order exponential curve.

3. Methods

3.1 Synthesis of chiral *sp²C*-COF and its film

Dialdehydes (0.125 mmol, terephthalaldehyde for TT-COF or 4,4'-biphenyldicarboxaldehyde for TB-COF) and (R/S)-1-phenethylamine (30 mg, 0.25 mmol, 1 equiv.) were combined in a vial with a mixture of mesitylene and dioxane (0.9 mL, 1:1 v/v). The mixture was sonicated for 5 min to afford a homogeneous solution, followed by the addition of 2,4,6-trimethyl-1,3,5-triazine (TMT, 10.26 mg, 0.083 mmol) and acetonitrile (0.025 mL). The obtained solution was transferred into a Pyrex tube, and trifluoroacetic acid (TFA, 0.2 mL) was added as a catalyst. The tube was subjected to three freeze–pump–thaw cycles for degassing and then sealed under vacuum. The reaction was carried out in an oven at 60°C for 7 days. The solid product was collected by filtration, neutralized with TEA (5×5 mL), washed with THF (5×5 mL), Soxhlet-extracted with THF for 24 h, and dried at 40°C under vacuum overnight to yield a yellow solid (85%-91%). Achiral sp^2C-COFs were synthesized analogously without adding (*R*/*S*)-1-phenethylamine. (Rac)-*sp²*C-COFs were synthesized using (*Rac*)-1-phenethylamine. The same procedure was also employed to prepare chiral COF films on substrates by placing the substrate inside the Pyrex tube prior to the reaction.

3.2 Post treatment of chiral *sp*^{2}C-COF

The as-synthesized chiral *sp*^{2}C-COFs was post treated under the solvothermal conditions. 20 mg chiral *sp*^{2}C-COF was charged into a Pyrex tube (10 cm×1cm) and added with a mixture of mesitylene and dioxane (1.5 mL, v/v, 1/1). Then 0.3 mL trifluoroacetic acid was added to the mixture. After three freeze-pump-thaw cycles, the tube was sealed off and kept in oven at 120℃ for 3 days. Afterward, the precipitate was filtered, neutralized by TEA (5×5 mL), washed with THF (5×5 mL), extracted by Soxhlet with THF for 24 h, and dried under vacuum at 40℃ for 24 h.

3.3 Chirality-induced synthesis of *sp*^{2}C-COF with a base catalyst

The procedure was modified from the reported solvothermal method for TT-COF through the base-catalyzed Adol condensation.[S1] A small vial was charged with terephthalaldehyde (16.77 mg, 0.125 mmol) for TT-COF, (*R*)-1-phenethylamine (30 mg, 0.25 mmol, 1 *eq.*), and a mixture of ethanol and dioxane (1.0 mL, 2:3 v/v). The mixture was sonicated for 5 min to give a yellow solution, followed by the addition of 2,4,6-trimethyl-1,3,5-triazine (TMT) (10.26 mg, 0.083 mmol). The obtained solution was transferred into a Pyrex tube. Then 1M NaOH aqueous solution (0.2 mL) was added to the mixture as a catalyst. The tube was degassed by three freeze–pump–thaw cycles and sealed off. Then the reaction proceeded in an oven at 100°C for 3 days. The precipitate was filtered off, washed with water (3×10 mL) and THF (5×10 mL), extracted by Soxhlet with THF for 24 h, and dried at 40^{o}C under vacuum overnight to give the yellow product with a yield of 90%.

3.4 Fabrication of TT(Δ)-COF/PDMS film

The ethyl acetate dispersion of TT(Δ)-COF (50 mg/L, 0.5 mL) were mixed with the solution of PDMS (5.0 g) and cross-linker (0.5 g). The mixture was stirred for 3 h to remove excess ethyl acetate, forming a uniform dispersion. Then it was

transferred to a mold and stood for 30 min in vacuum. After being cured at 80°C for 14 h, the transparent and flexible TT(Δ)-COF/PDMS film was obtained.

3.5 Photoelectrochemical (electrochemical) measurement

The photocurrent response profiles and electrochemical impedance spectra were tested by the CHI 760E electrochemical workstation with a standard three-electrode system, using the Ar purged 0.1M Na_2SO_4 (pH=6.8) as the electrolyte, sample-coated ITO as the working electrode, Pt wire as the counter electrode and Ag/AgCl electrode as the reference electrode. The 300 W Xe lamp (AM1.5G) with a power density of 100 mW·cm^{-2} was used as the light source.

The conversion between potentials *vs.* Ag/AgCl, those *vs.* RHE and those *vs.* NHE follows the equation below:

$$E(vs.\,RHE) = E(vs.Ag/AgCl) + E_{Ag/AgCl} + 0.059V \times pH \quad (1)$$

$$E(vs.\,NHE) = E(vs.Ag/AgCl) + E_{Ag/AgCl} \quad (2)$$

($E_{Ag/AgCl}$=0.1967 V *vs.* NHE at 25 ℃)

3.6 Performance evaluation of COF-modified interdigitated capacitive sensor

The sensing performance of the COF-modified interdigital capacitive sensor was evaluated at room temperature. The sensor was immersed in the sample solution for 30 seconds, after which the capacitance was measured using an M4070 LCR meter (Jingyan Instruments, China). Tryptophan in ethanol was used as the analyte. To ensure reproducibility, the measurements were repeated across three independent tests. The results showed a standard deviation of less than 1%, confirming good reproducibility and reliability of the sensing system. According to the literature,[S2] the selectivity factor was calculated using the control sample of ethanol.

3.7 Synthesis of model compounds

2, 4, 6-tri(4-vinylbenzoyl)-s-triazine

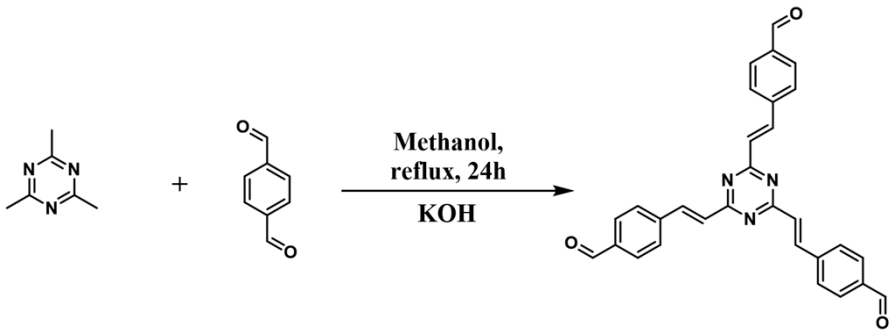

1,4-Phthalaldehyde (400 mg, 3 mmol), KOH (170 mg, 1 mmol) and methanol (25 mL) were mixed in a 150 mL round-bottom flask. Then trimethyl-s-triazine (123.2 mg, 1 mmol) was dissolved in 25 mL methanol and the solution was added into the mixture. The reaction proceeded under reflux for 24 h. The solid product was collected by filtration and washed thoroughly with methanol and water. The crude product was purified by silica gel column chromatography using mixed solvents [v (ethyl acetate) : v (petroleum ether) = 1 : 1] as the first eluent and dichloromethane as the second eluent. The yellowish product was obtained after drying under vacuum for 24 h (0.283 g, 0.60 mmol, 60%). ^{1}H NMR (400 MHz, $CDCl_3$): δ 10.06 (s, 3H), 8.32 (d, 3H), 7.96 (d, 6H), 7.84 (d, 6H) and 7.33 (d, 3H). ^{13}C NMR (400 MHz, $CDCl_3$): δ 191.50, 171.09, 141.01, 140.42, 136.99, 130.28, 129.18, 128.59.

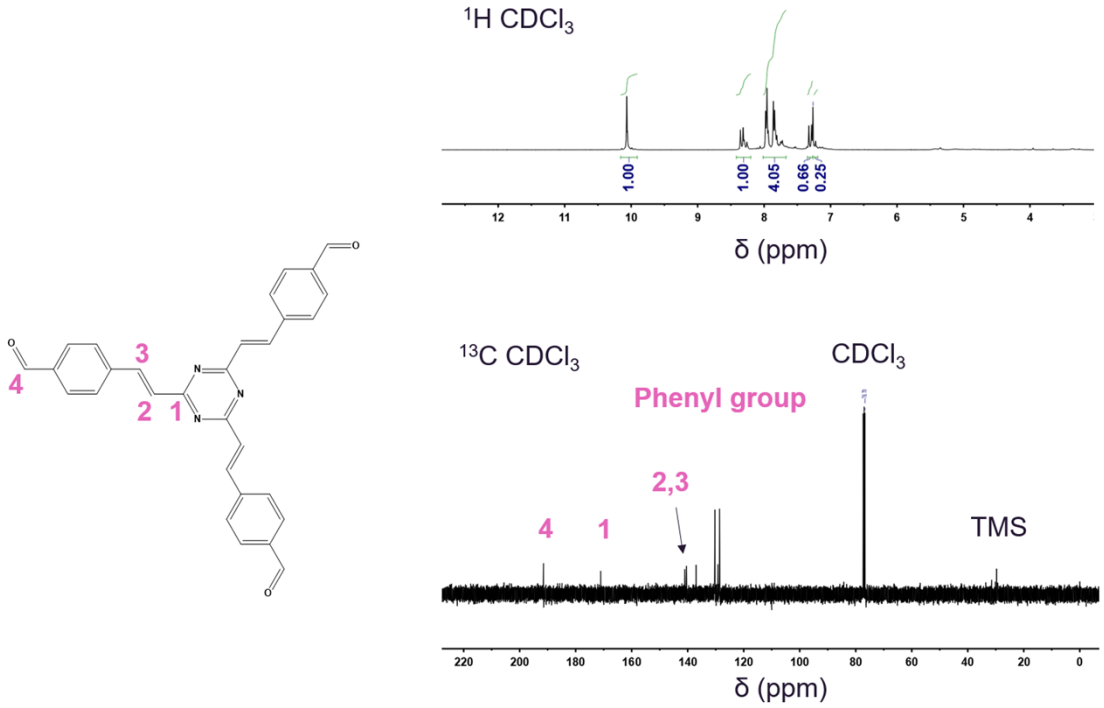

(*R*)-model compound

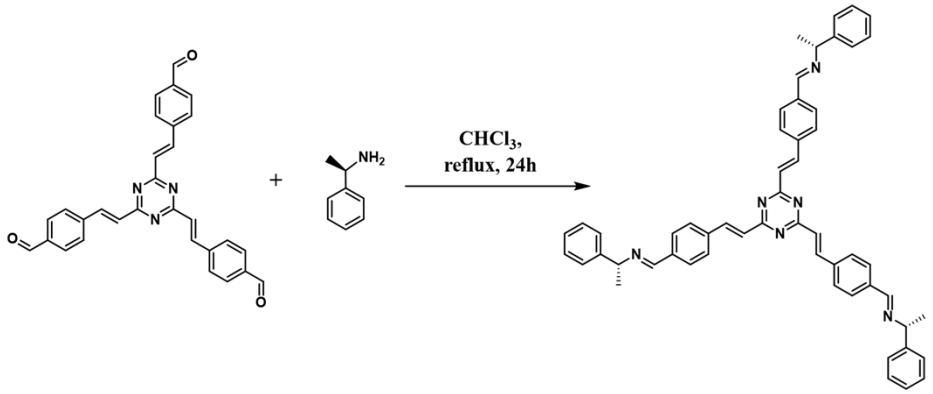

2, 4, 6-tri(4-vinylbenzoyl)-s-triazine (94 mg, 0.2 mmol), (*R*)-phenethylamine (144 mg, 1.2 mmol) and chloroform (30 mL) were mixed in a 100 mL round-bottom flask. The reaction proceeded under reflux for 24 h. After rotary evaporation, the solid product was washed with methanol for several times and collected by filtration. The orange product was obtained after drying under vacuum for 24 h (0.153 g, 0.20 mmol, 98%). The needle-like single crystal was obtained in the mixed solvent of toluene and cyclohexane after 2 months. ^{1}H NMR (400 MHz, $CDCl_3$): δ 8.37 (s, 3H), 8.27 (d, 3H), 7.83 (d, 6H), 7.70 (d, 6H), 7.44 (d, 6H), 7.36 (d, 6H), 7.27 (d, 3H), 7.17 (d, 3H), 4.56 (m, 3H) and 1.61 (d, 9H). ^{13}C NMR (400 MHz,

$CDCl_3$): δ 171.19, 158.73, 145.04, 141.00, 137.66, 137.50, 128.79, 128.49, 128.32, 127.22, 126.93, 126.65, 69.90, 24.90.

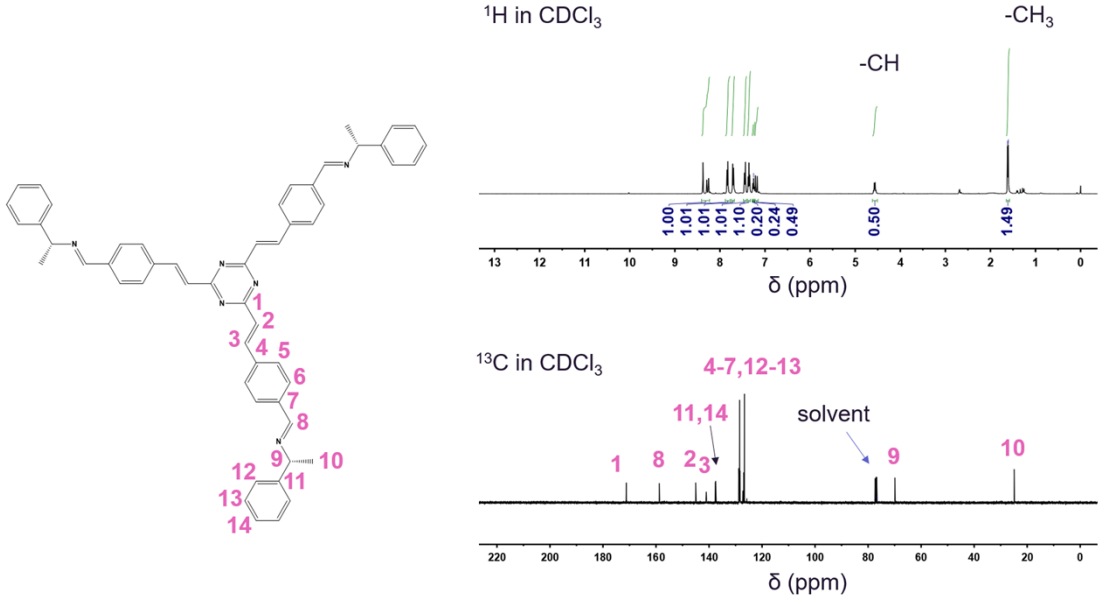

(*S*)-model compound

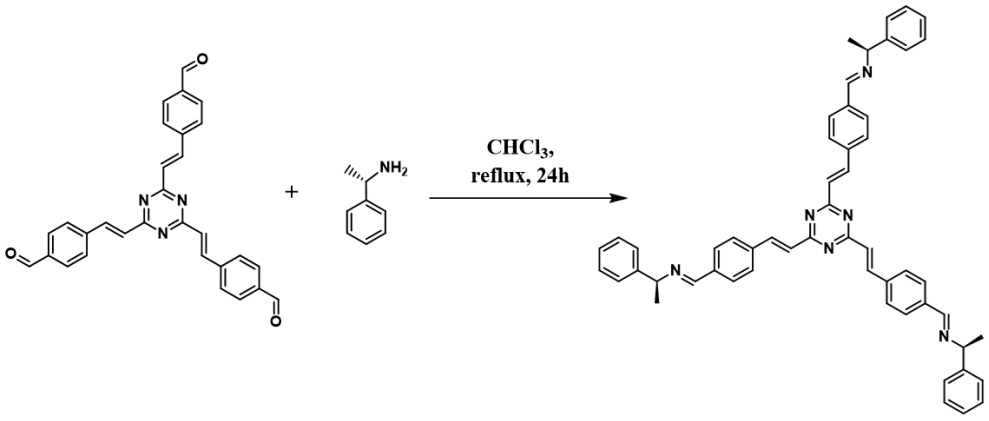

2, 4, 6-tri(4-vinylbenzoyl)-s-triazine (94 mg, 0.2 mmol), (*S*)-phenethylamine (144 mg, 1.2 mmol) and chloroform (30 mL) were mixed in a 100 mL round-bottom flask. The reaction proceeded under reflux for 24 h. After rotary evaporation, the solid product was washed with methanol for several times and collected by filtration. The orange product was obtained after drying under vacuum for 24 h (0.151 g, 0.20 mmol, 97%). ^{1}H NMR (400 MHz, $CDCl_3$): δ 8.40 (s, 3H), 8.29 (d, 3H), 7.85 (d, 6H), 7.72 (d, 6H), 7.45 (d, 6H), 7.36 (d, 6H), 7.27 (d, 3H), 7.19 (d, 3H), 4.58

(m, 3H) and 1.62 (d, 9H). ^{13}C NMR (400 MHz, $CDCl_3$): δ 171.23, 158.73, 145.04, 141.05, 137.69, 137.51, 128.80, 128.49, 128.34, 127.23, 126.94, 126.66, 69.92, 24.89.

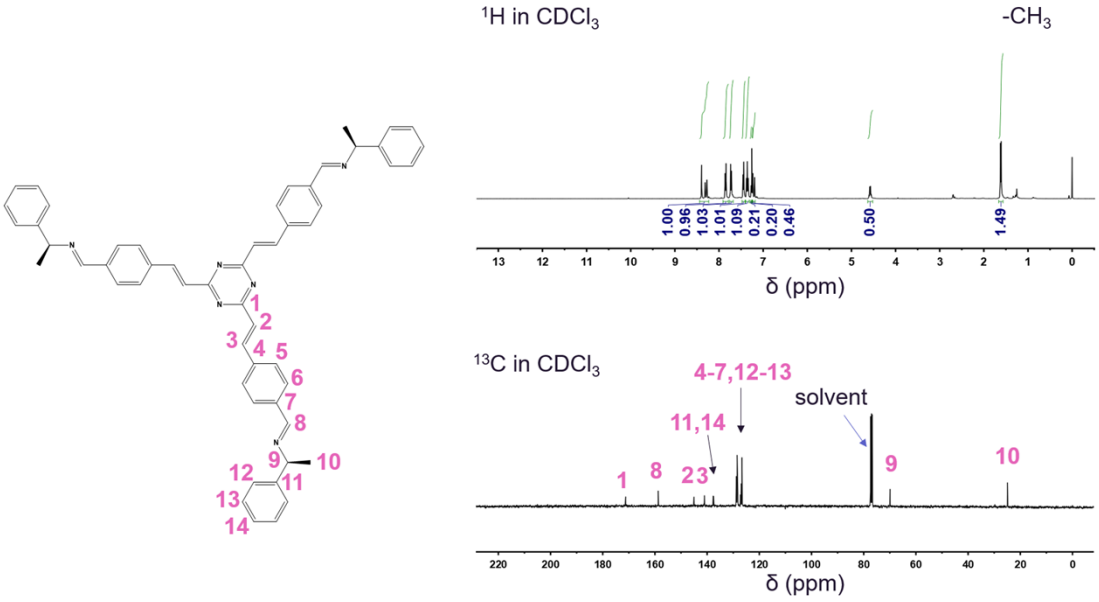

3.8 DFT Calculations

The DFT calculation was performed by Gaussian 16 software package.[S3] The models for the reaction pathway calculation were completely optimized at the PBE0-D3BJ/def2-TZVP level.[S4,S5] The vibrational frequency calculation was carried out at the same level of theory. The transitional state was obtained by the Berny method and exhibited only one imaginary frequency. In the calculation of the electronic circular dichroism, C and N atoms were directly cut from the refined crystal structure without further relaxation, while H atoms were optimized at the level of PBE0-D3BJ/def2-SVP. Then the vertical excitation calculations were performed at TD-PBE0-D3BJ/def2-SVP level for at least 30 states. The simplified TD-DFT calculation[S6] of the extended macrocycles was carried out using ORCA 5.0.3,[S7] based on the ωB97X-D3/ def2-SVP level[S8] with RI-J and COSX algorithm.[S9] The electron-hole analysis was processed using Multiwfn 3.8[S10] and visualized by VMD 1.9.3 package.[S11] The spontaneous emission rate was calculated by the following equation:[S12]

$$\tau = \frac{3}{2fv^2}$$

where τ stands for lifetime (s) of the excited state, *f* presents the oscillator strength, *v* presents the transition energy (cm^{-1}), and spontaneous emission rate (s^{-1}) is the reciprocal of lifetime.

The crystal structures were modelled by CP2K package[S13] in a full relaxation. In the cell relaxation, the mixed Gaussian and plane waves (GPW) method was applied using the Perdew-Burke-Ernzerhof (PBE) exchange-correlation functional with the DFT-D3(BJ) dispersion correction, based on the GTH pseudopotentials with DZVP-MOLOPT-SR gaussian and plane wave basis set with the cutoff of 600 Ry mapped on a 4-level multigrid. The relative cutoff was set to 50 Ry with the progression factor of 3. The efficient orbital transformation (OT) method and Quickstep code were used to accelerate the calculation. All the structures were optimized by the Broyden-Fletcher-Goldfarb-Shanno (BFGS) minimizer, and the SCF convergence criterion was set to 5×10^{-7} to increase the accuracy of density matrix.

Section II. Figures and Tables

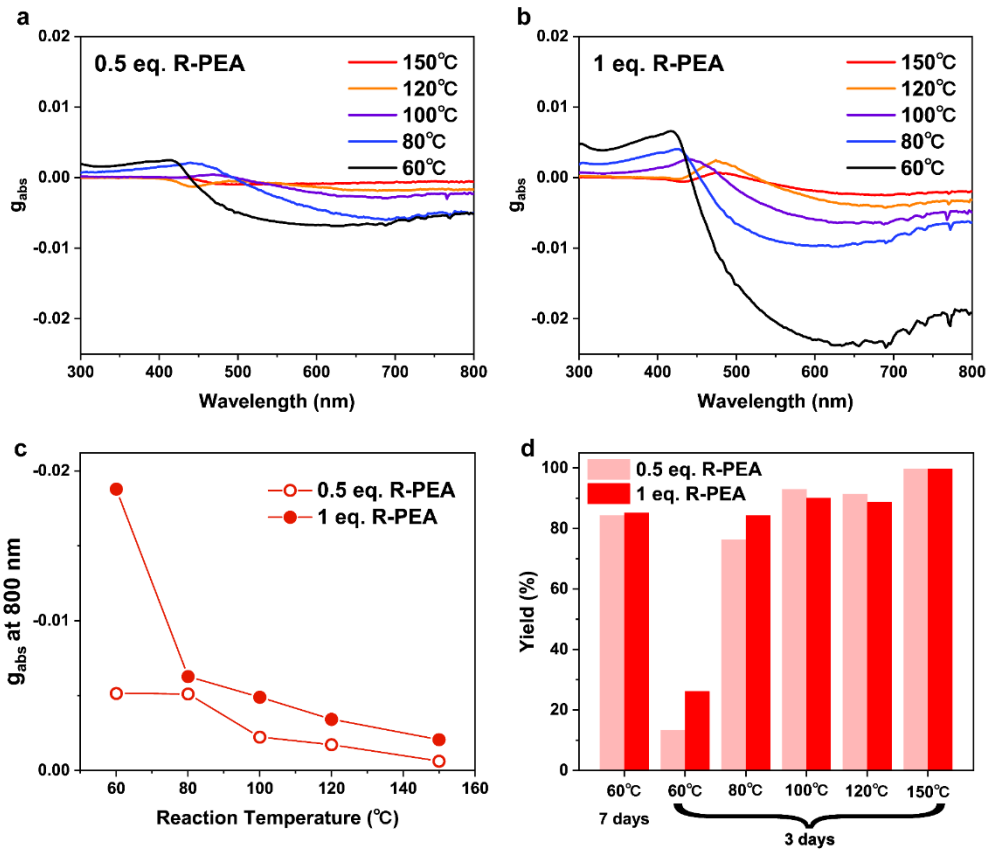

Fig. S1 (a-c) The effect of reaction temperatures on the absorptive dissymmetry factor (g_{abs}) of chiral TT(Δ)-COF synthesized for 3 days. **(d)** The effect of different reaction conditions on the yield of chiral TT(Δ)-COF.

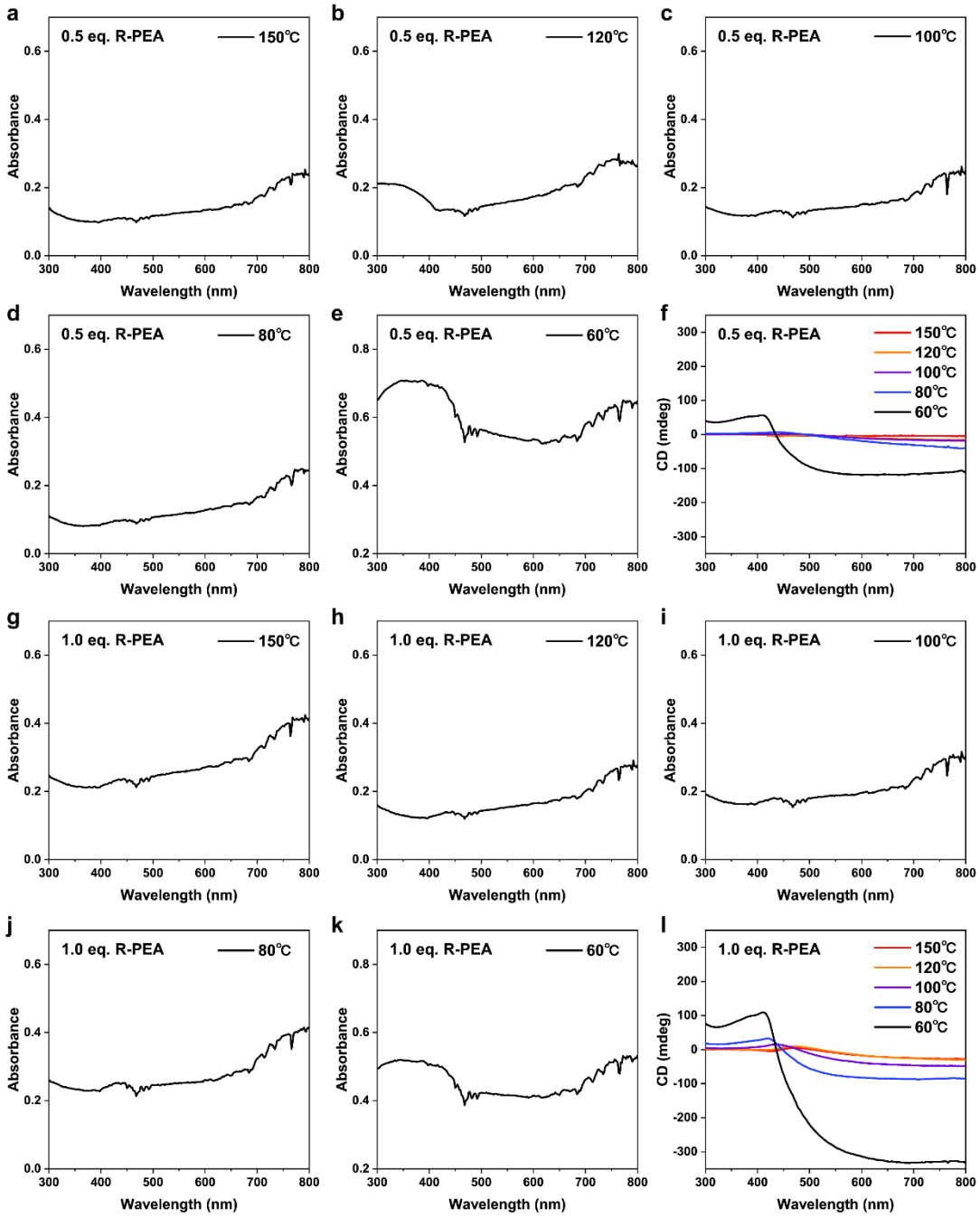

Fig. S2 (a-f) The UV-vis spectra (a-e) and circular dichroism spectra (f) of chiral TT(Δ)-COF synthesized with 0.5 eq. *R*-PEA at varied temperatures for 3 days. (g-l) The UV-vis spectra (g-k) and circular dichroism spectra (l) of chiral TT(Δ)-COF synthesized with 1 eq. *R*-PEA at varied temperatures for 3 days.

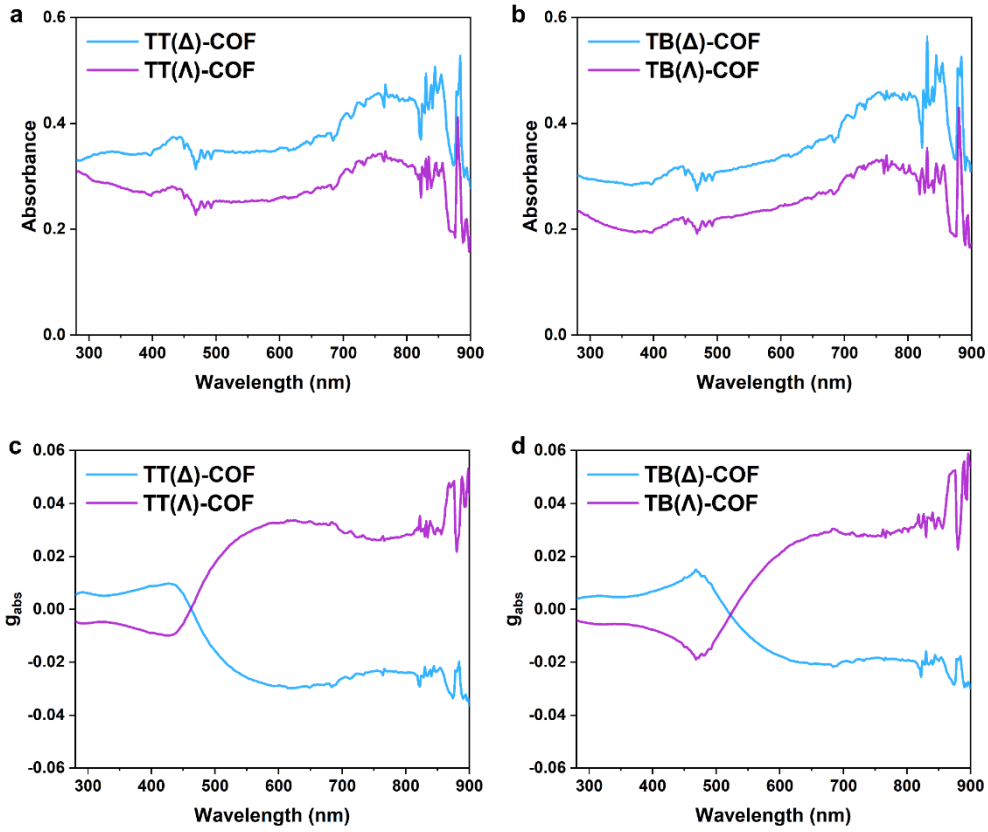

Fig. S3 (a,b) UV-vis spectra and (c,d) the corresponding asymmetry factor (g_{abs}) of TT(Δ)/(Λ)-COF and TB(Δ)/(Λ)-COF. The absorption peaks of TT-COF and TB-COF are mainly attributed by π→π* transition.

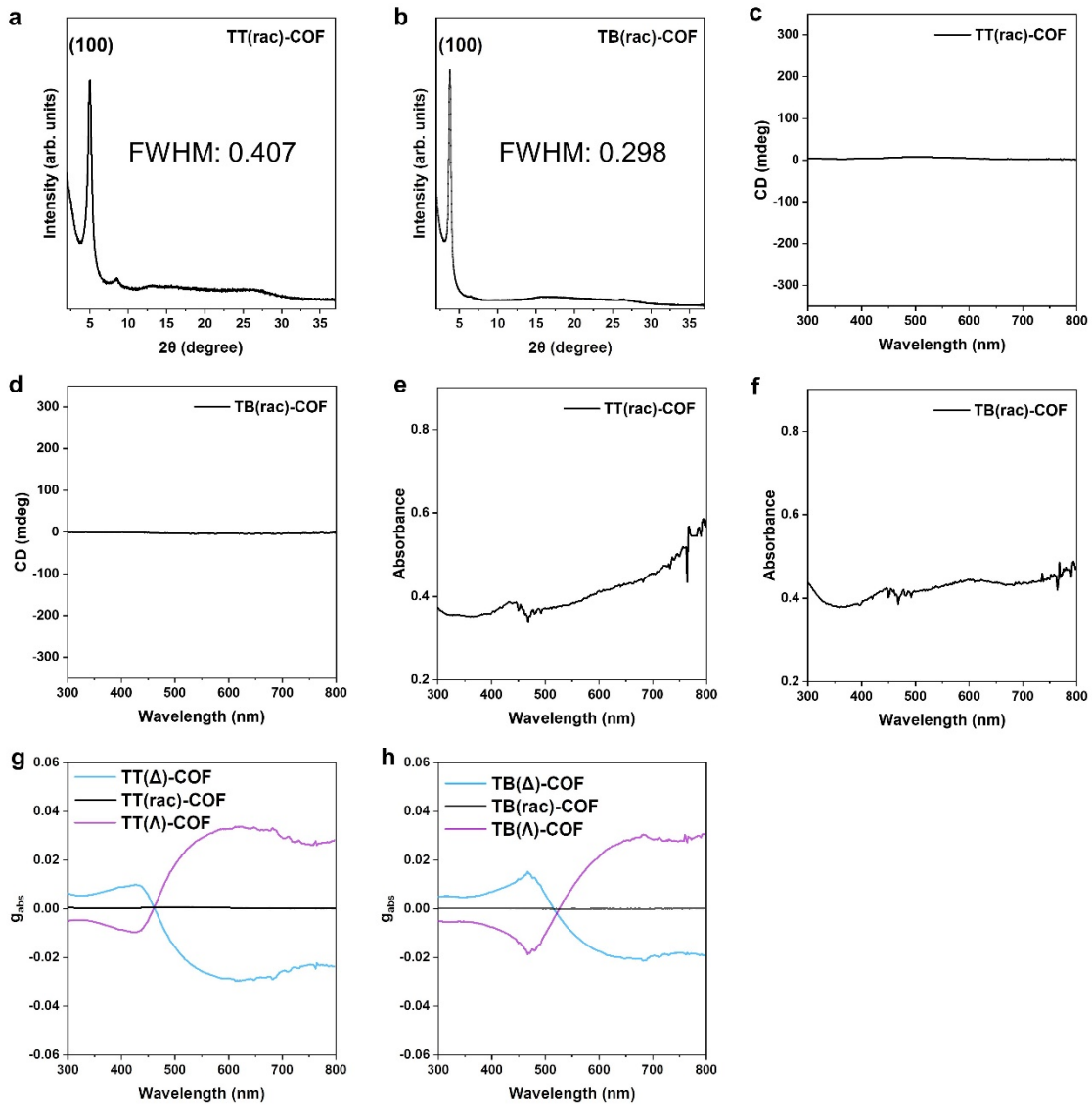

Fig. S4 (a,b) WAXS patterns of the TT(*rac*)-COF and TB(*rac*)-COF, with the calculated FWHM of (100) peak. (c,d) Circular dichroism spectra, (e,f) UV-vis spectra and (g,h) the corresponding asymmetry factor of TT(*rac*)-COF and TB(*rac*)-COF.

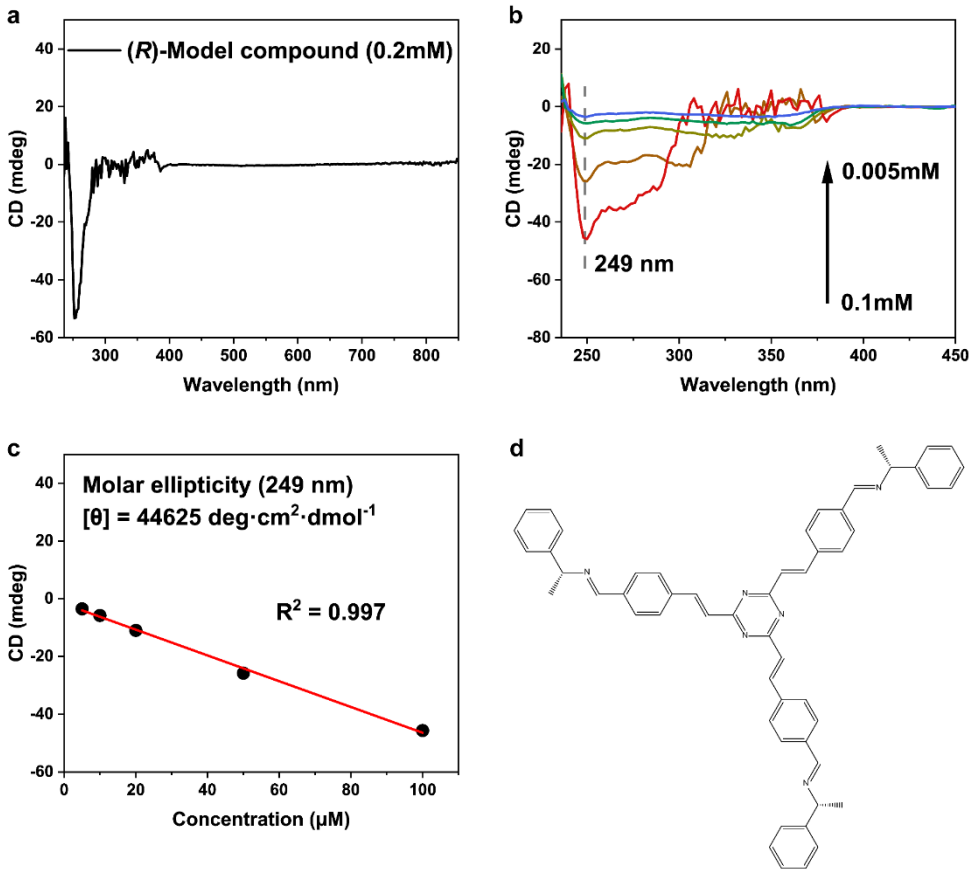

Fig. S5 (a) Circular dichroism spectrum of the (*R*)-model compound (0.2mM in $CHCl_3$). (b) Circular dichroism curves of the (*R*)-model compound with various concentrations. (c) The derived molar ellipticity of the (*R*)-model compound. (d) The structure of (*R*)-model compound.

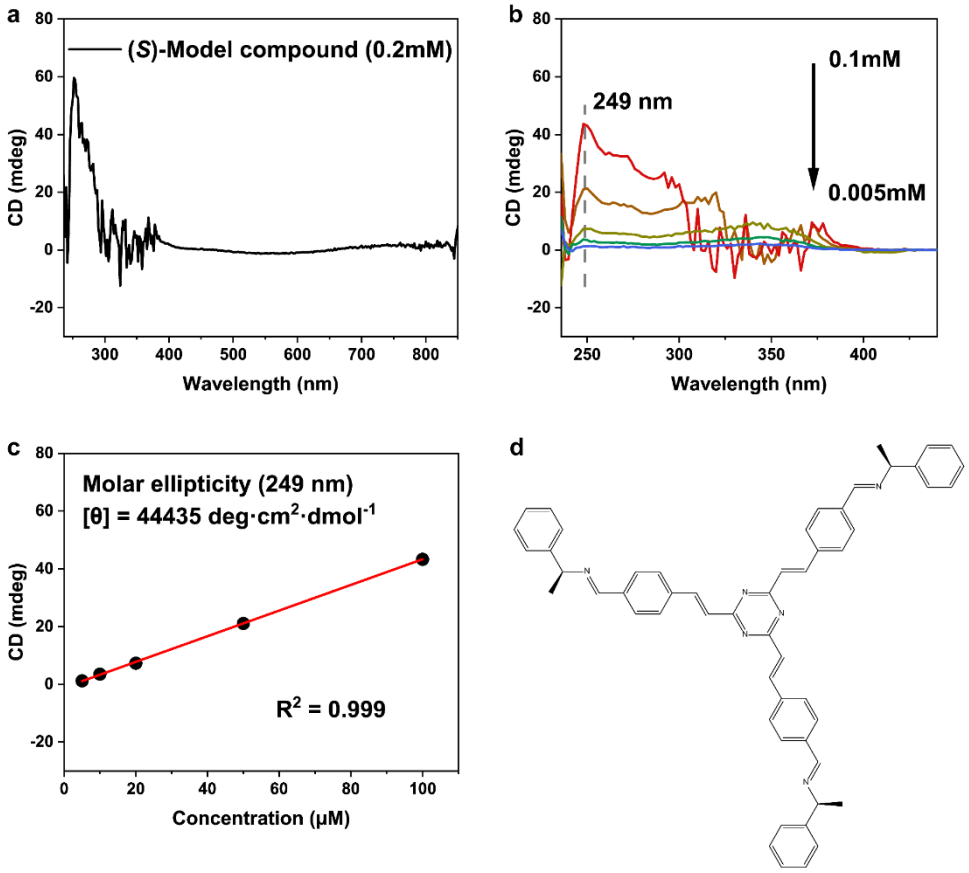

Fig. S6 (a) Circular dichroism spectrum of the (*S*)-model compound (0.2mM in $CHCl_3$). (b) Circular dichroism curves of the (*S*)-model compound with various concentrations. (c) The derived molar ellipticity of the (*S*)-model compound. (d) The structure of (*S*)-model compound.

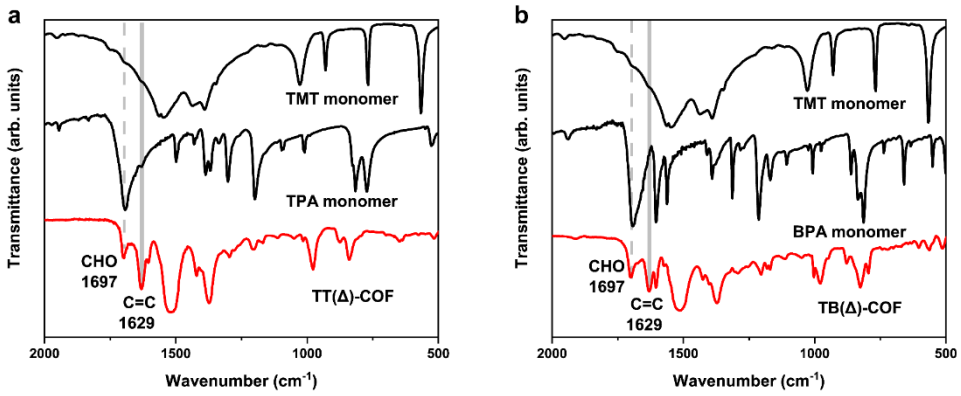

Fig. S7 FT IR spectra of (a) TT(Δ)-COF and (b) TB(Δ)-COF with the corresponding monomers.

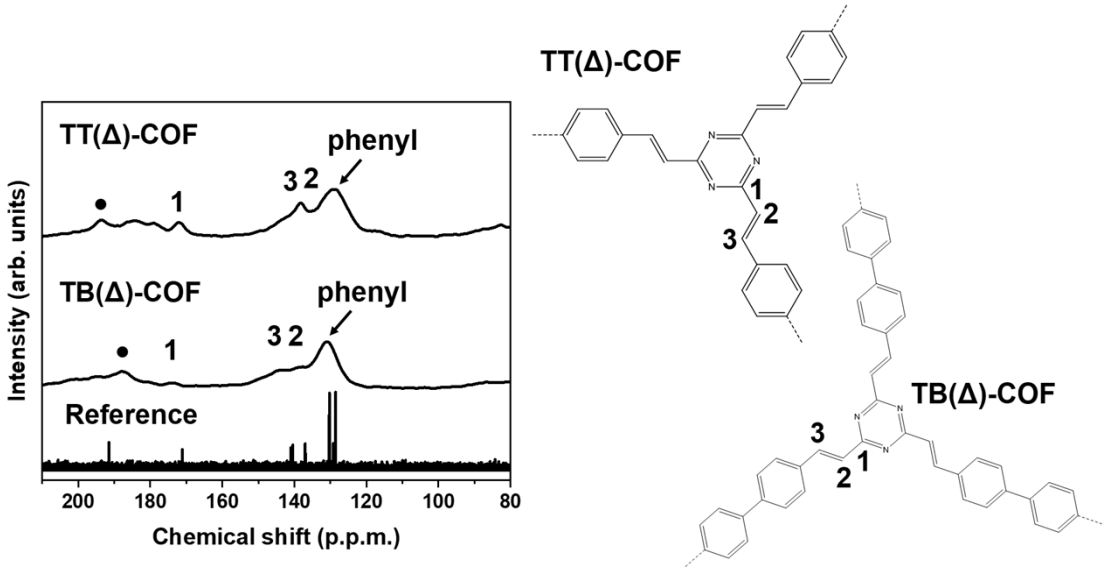

Fig. S8 Solid-state cross-polarization magic-angle-spinning ^{13}C NMR spectra of TT(Δ)-COF and TB(Δ)-COF. Reference is the ^{13}C NMR spectrum of 2, 4, 6-tri(4-vinylbenzoyl)-s-triazine in $CDCl_3$. (•) marks the chemical shift of residual aldehyde groups.

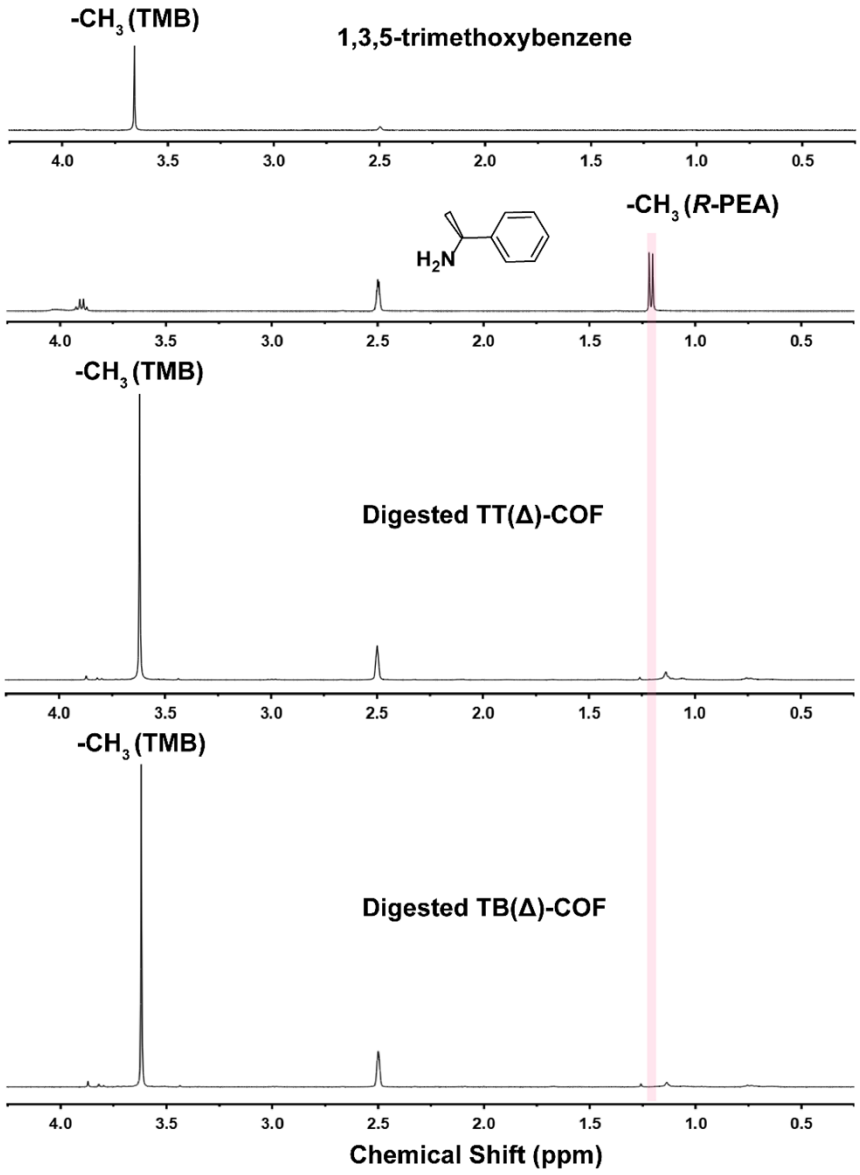

Fig. S9 The magnified ^{1}H NMR spectra of 1,3,5-trimethoxybenzene, *R*-1-PEA, digested TT(Δ)-COF and digested TB(Δ)-COF. For the complete cleavage of imine linkages, 10mg COF solid was dispersed in a mixture of NaOH in D_2O (0.11 mL, 10 mol/L) and DMSO-d6 (0.55 mL) and the mixture kept at 120^{o}C for 24h. After digestion, 2 mg 1,3,5-trimethoxybenzene (TMB) was added as the internal standard. The supernatant was subsequently isolated and subjected to NMR spectroscopic characterization.

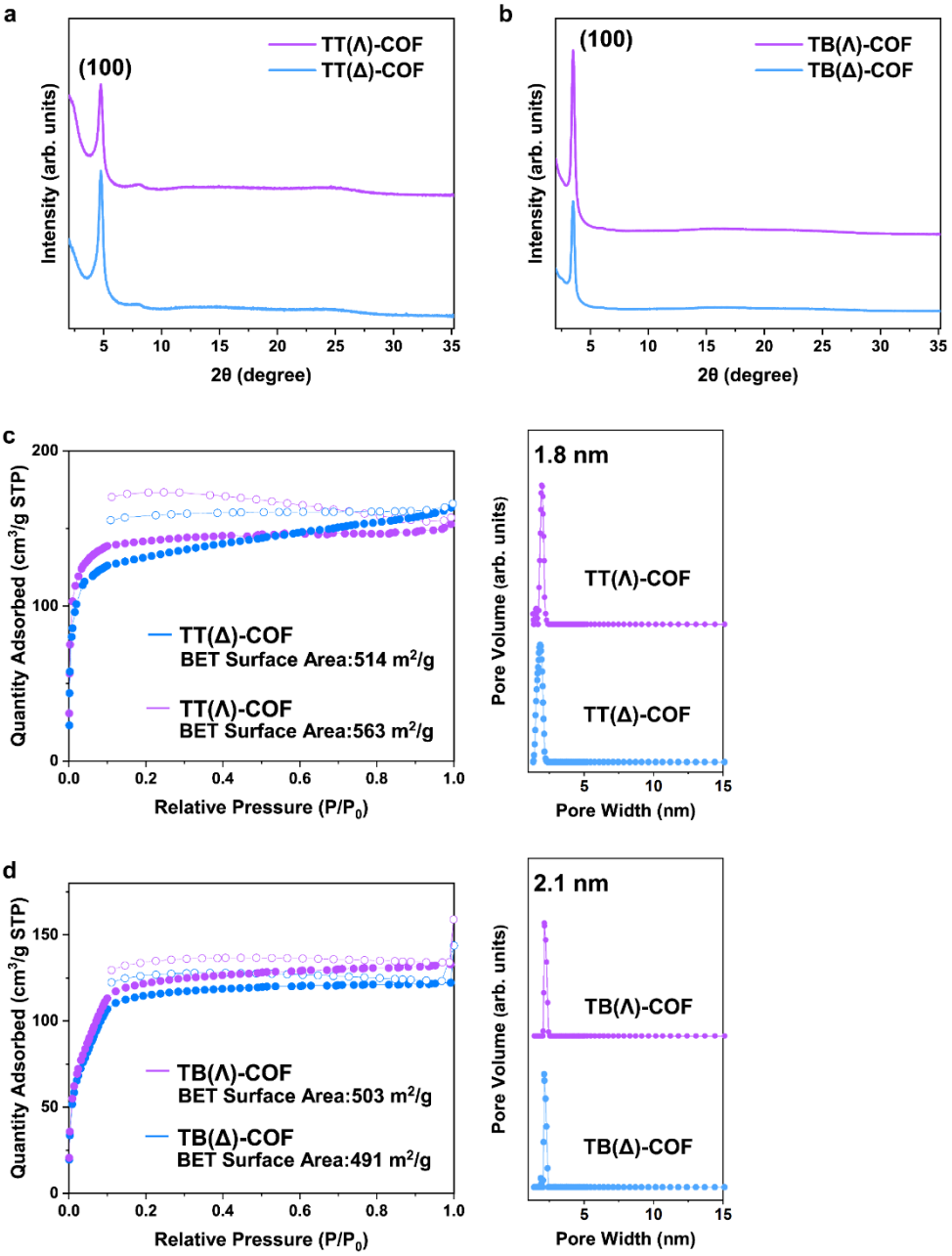

Fig. S10 (a,b) WAXS patterns and (c,d) N_2 sorption isotherms and pore-size distributions of TT(Δ)/(Λ)-COF and TB(Δ)/(Λ)-COF, respectively.

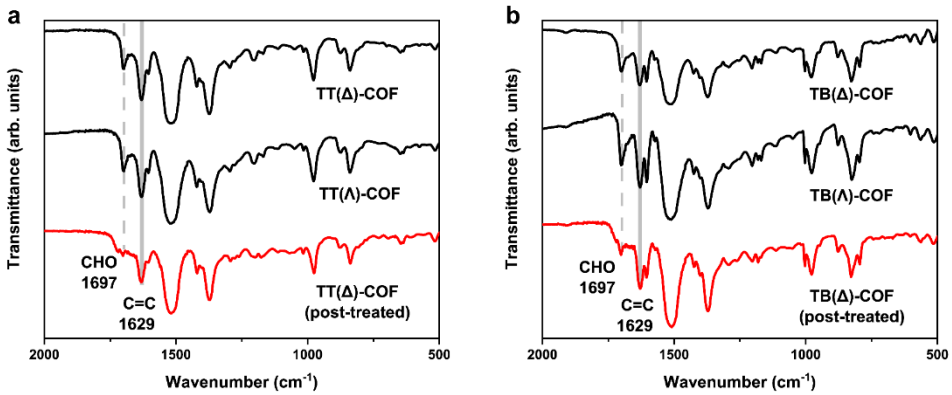

Fig. S11 (a) FT IR spectra of the TT(Δ)-COF, TT(Λ)-COF and post-treated TT(Δ)-COF. (b) FT IR spectra of the TB(Δ)-COF, TB(Λ)-COF and post-treated TB(Δ)-COF.

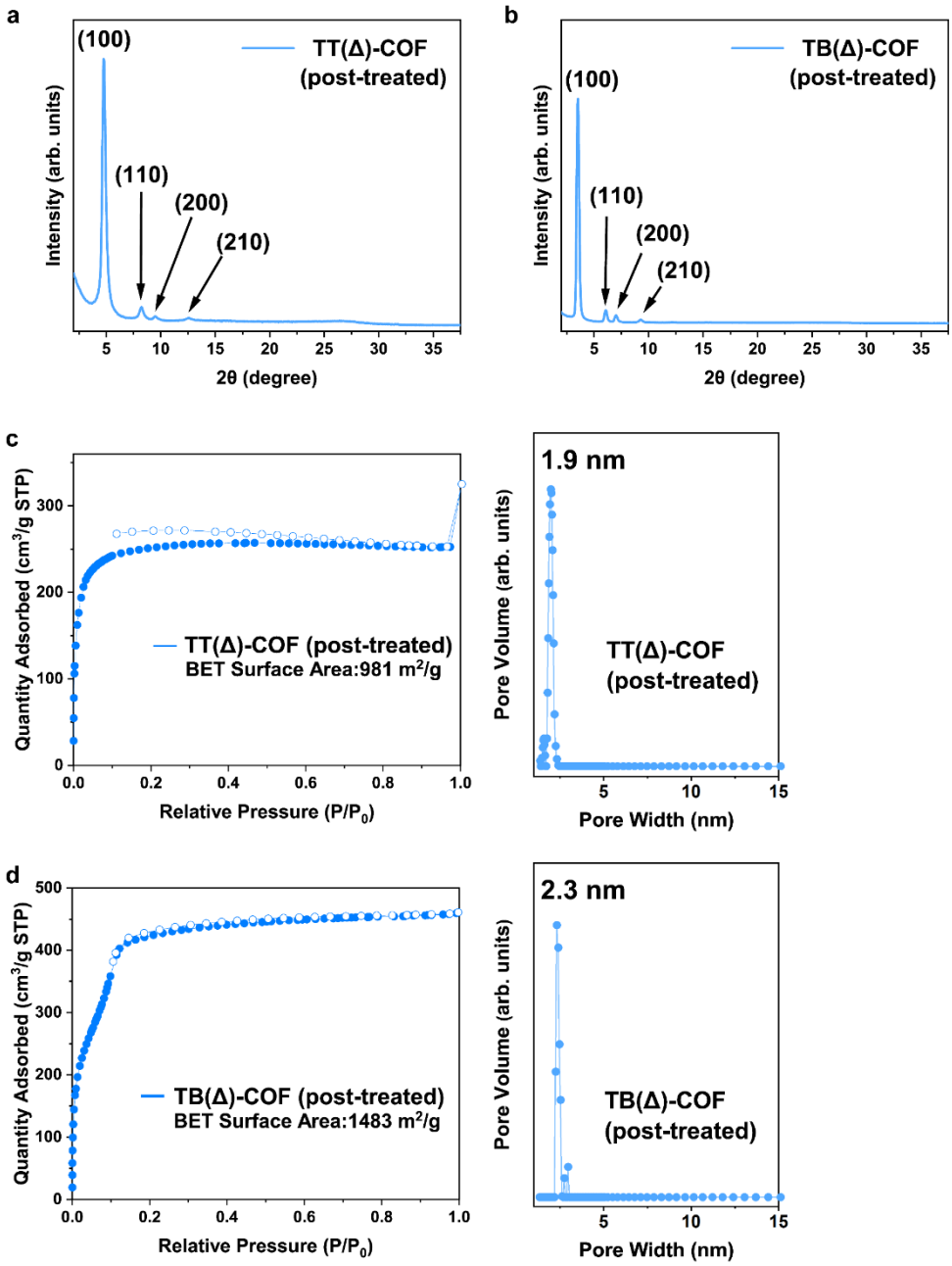

Fig. S12 (a,b) WAXS patterns and (c,d) N_2 sorption isotherms and the pore distributions of the post-treated TT(Δ)-COF and TB(Δ)-COF.

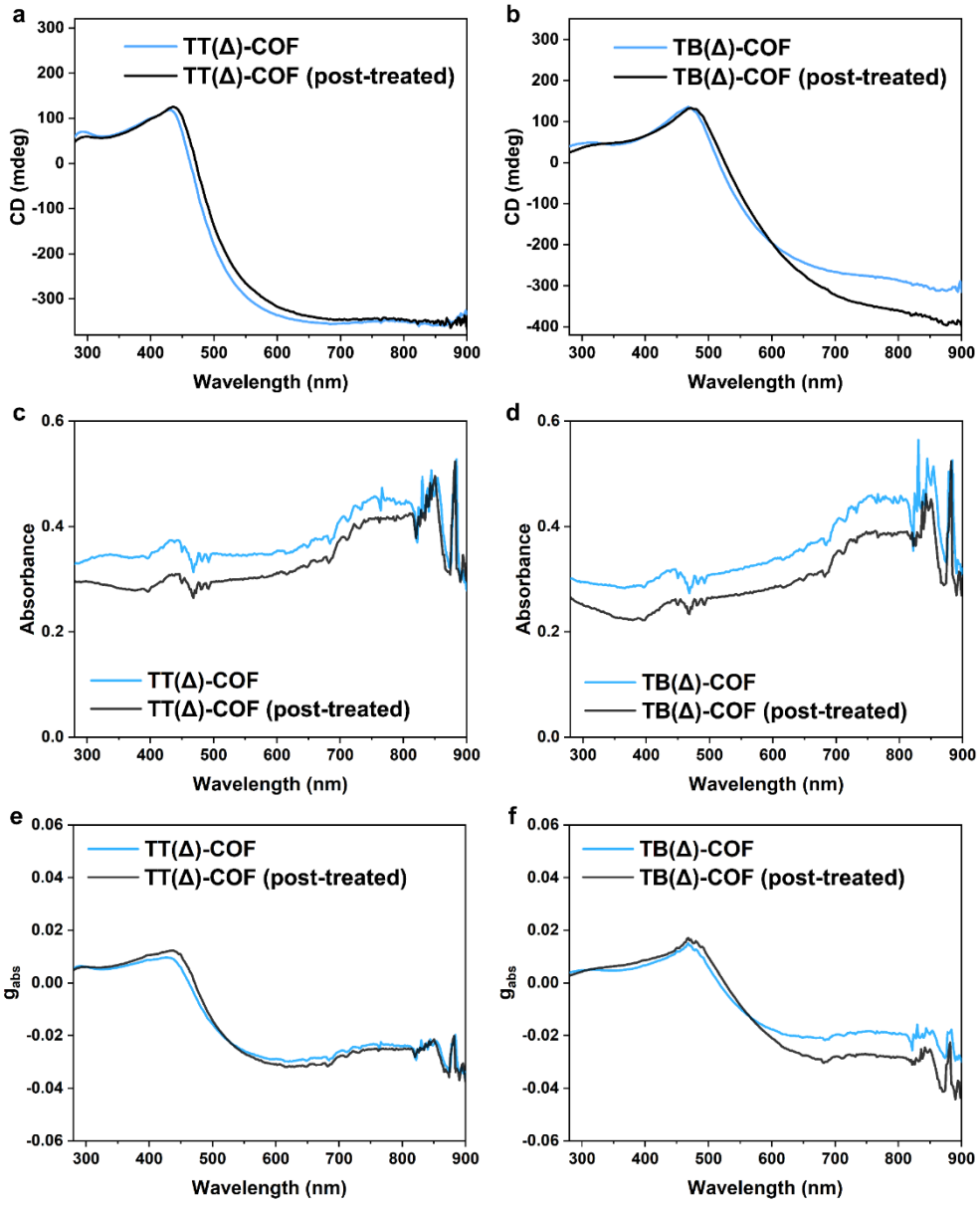

Fig. S13 (a,b) Circular dichroism spectra, (c,d) UV-vis spectra and (e,f) the corresponding asymmetry factor of the post-treated TT(Δ)-COF and TB(Δ)-COF.

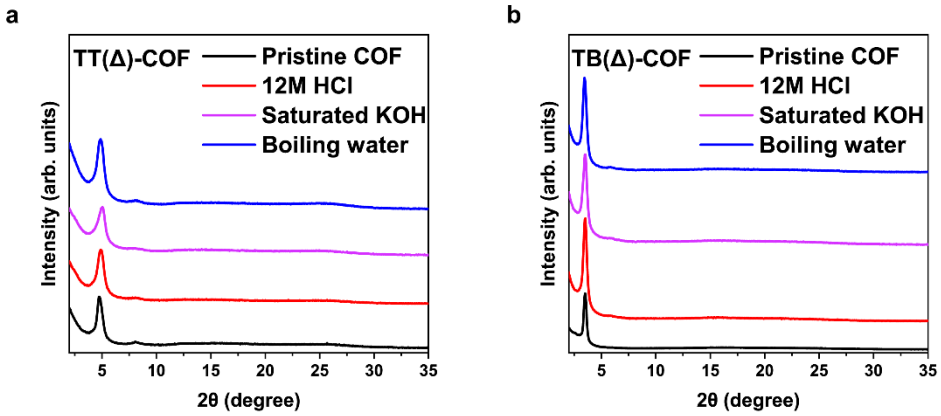

Fig. S14 (a,b) WAXS patterns of chiral (a) TT(Δ)-COF and (b) TB(Δ)-COF after 24 h harsh treatment in different conditions. After treatment with 12M HCl, the chiral sp^2C-COF was neutralized by ammonia water and washed by water and ethanol.

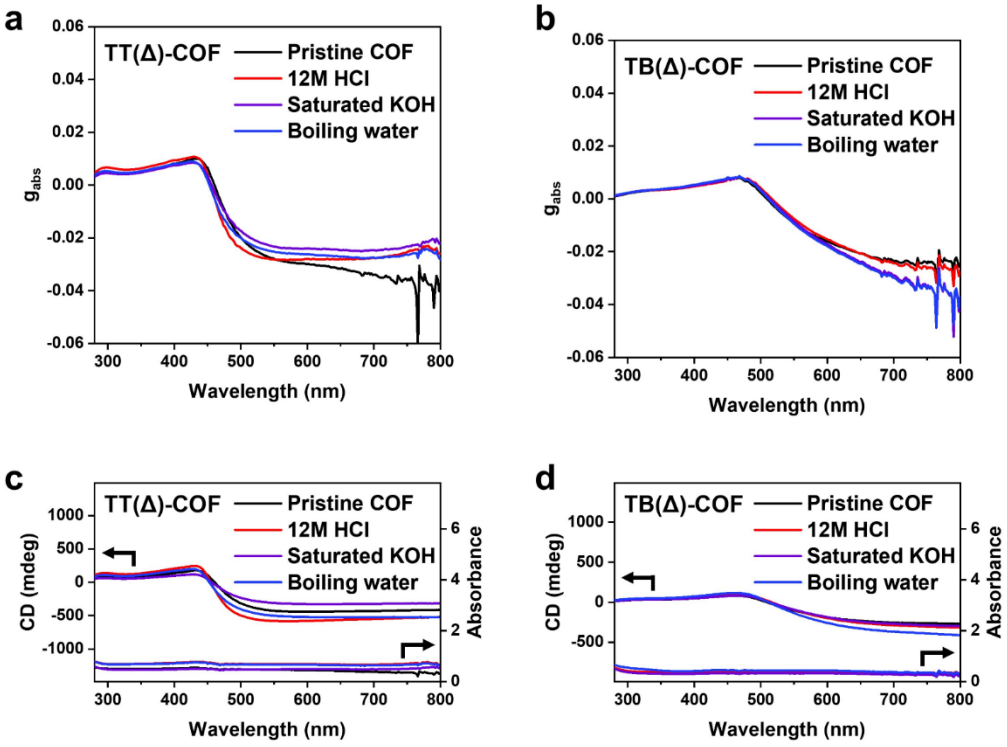

Fig. S15 (a,b) Absorptive dissymmetry factor (g_{abs}) of the post-treated chiral (a) TT(Δ)-COF and (b) TB(Δ)-COF. After treatment with 12M HCl, the chiral sp^2C-COF was neutralized by ammonia water and washed by water and ethanol. (c,d) The corresponding CD spectra and absorbance of the post-treated chiral (c) TT(Δ)-COF and (d) TB(Δ)-COF.

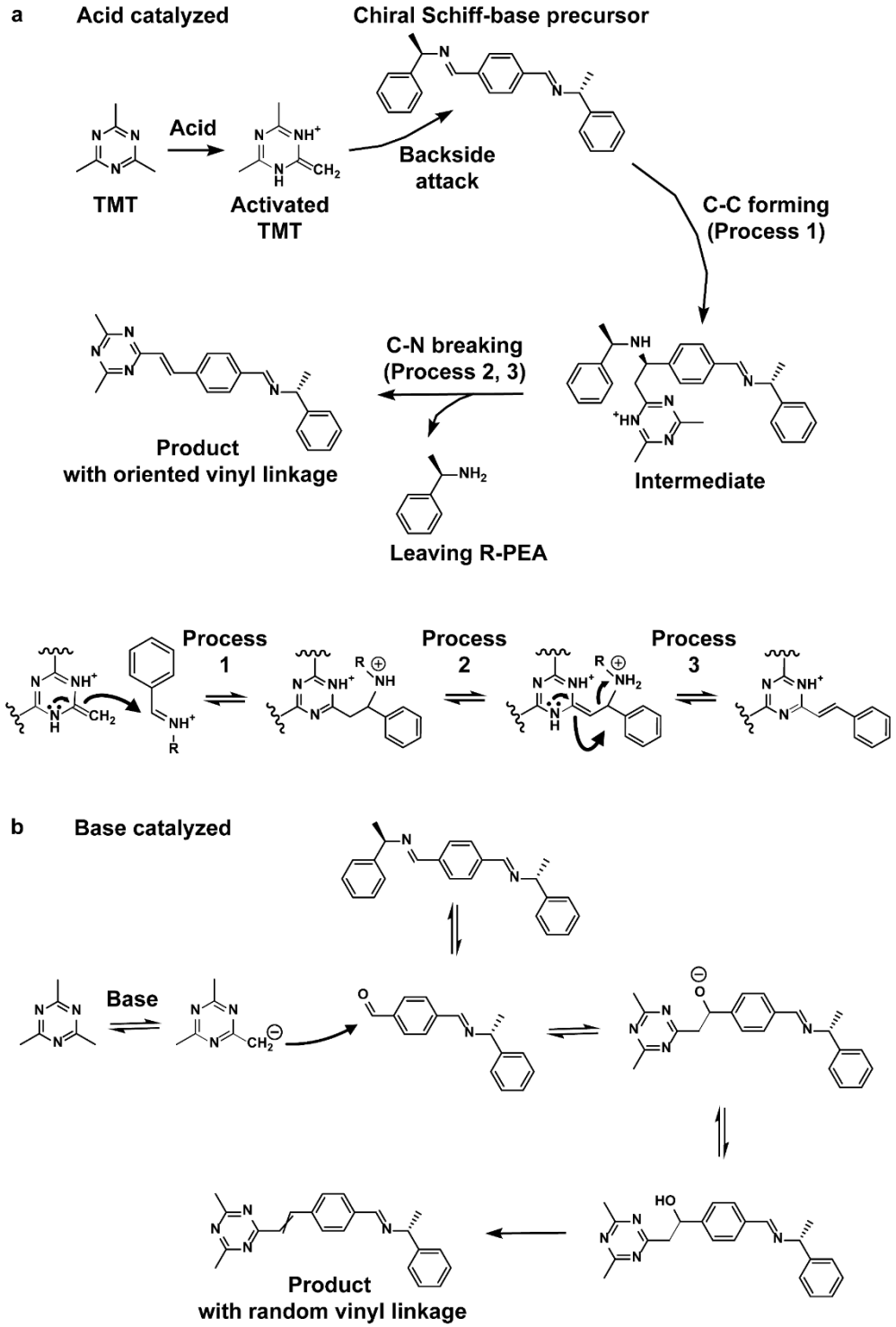

Fig. S16 Proposed mechanism of (a) acid-catalyzed and (b) base-catalyzed Aldol condensation in the presence of the chiral Schiff-base precursor.

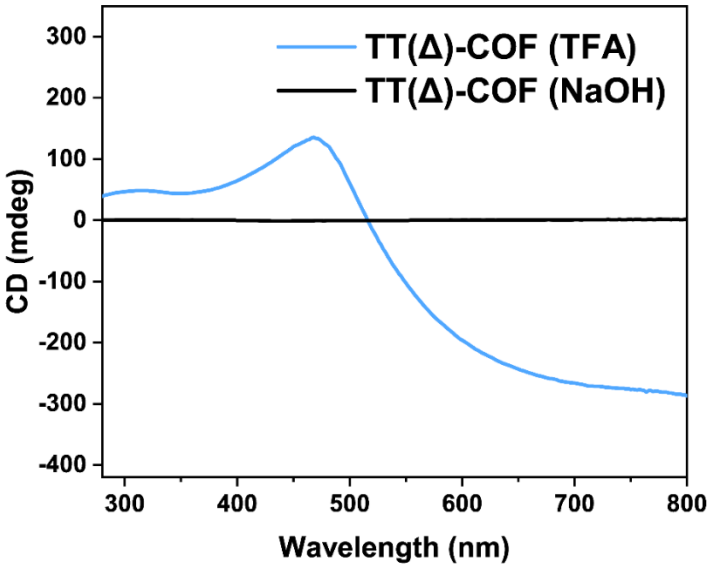

Fig. S17 Circular dichroism spectra of the TT(Δ)-COF synthesized using acid and base catalysts, respectively.

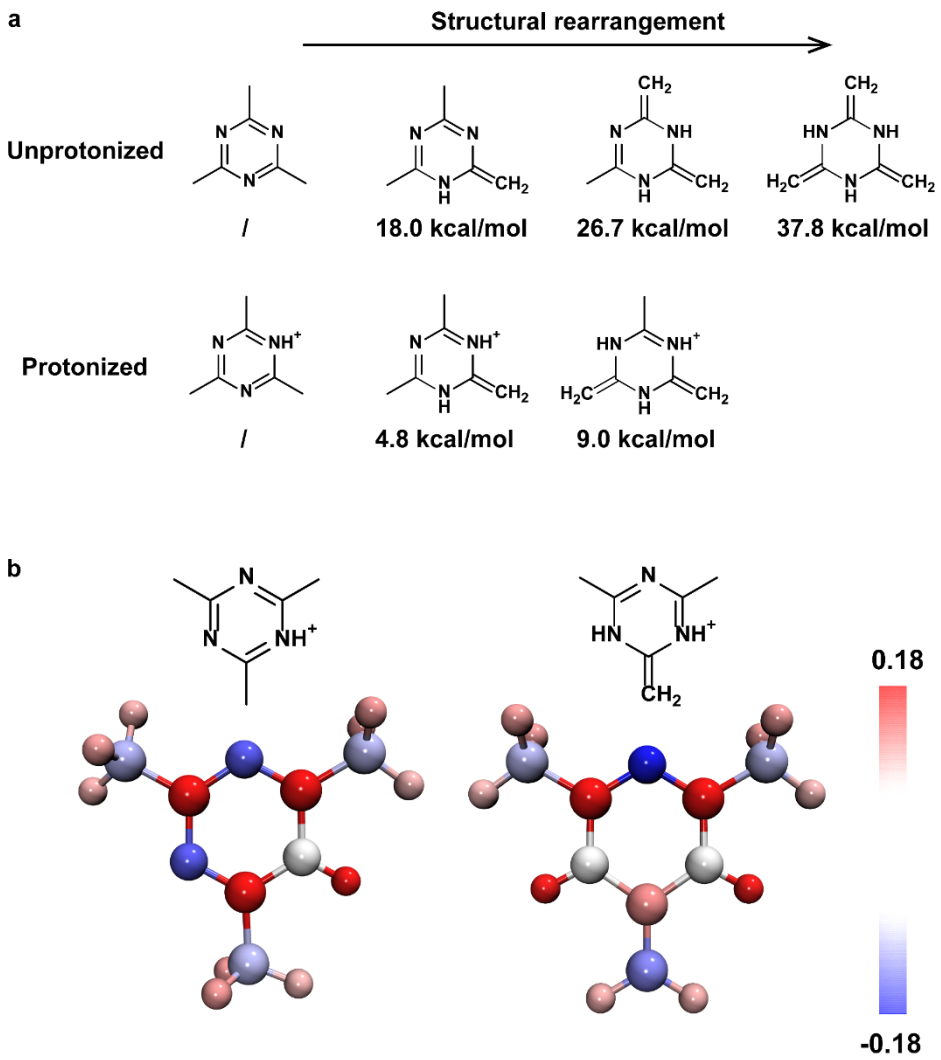

Fig. S18 (a) The calculated energy for the comparison of protonized and unprotonized TMT molecules after structural rearrangement, computed on PBE0-D3BJ/ def2-SVP level of theory ($E_{calculated}$ = $E_{rearraned}$ – E_{raw}). (b) The molecular structure of the rearranged TMT monomer, colored by the Hirshfeld atomic charge (red for positive charge and blue for negative charge).

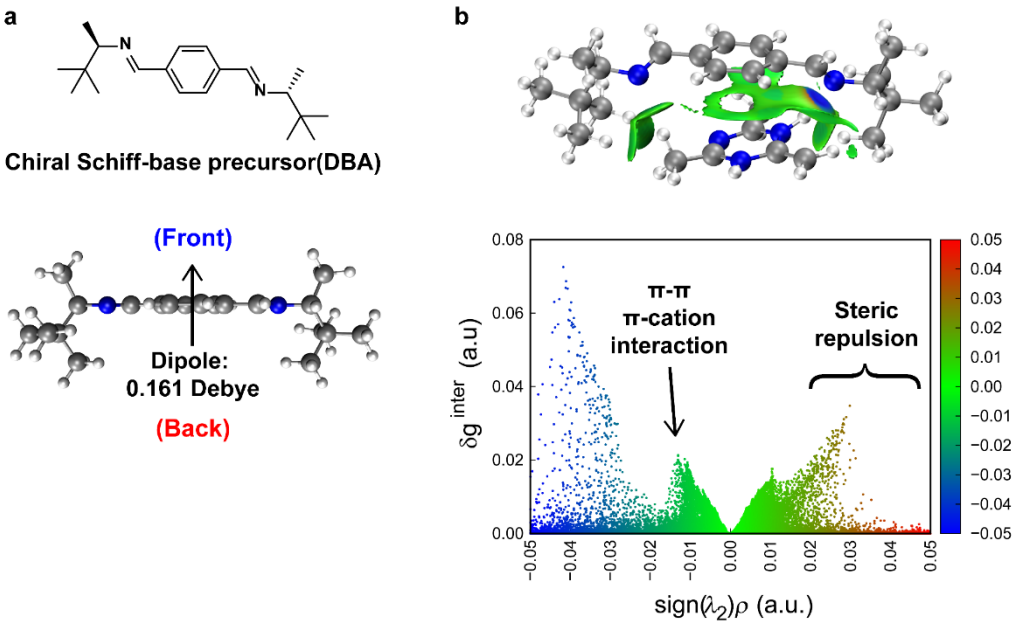

Fig. S19 (a) Structure of the chiral Schiff-base precursor with the dipole moment of 0.161 Debye, using (*S*)-(+)-3,3-dimethyl-2-butylamine (DBA). (b) IGMH scatter map of the transitional complex (DBA). The colored real-space presentation (isovalue = 0.005) is related to the weak interaction through the IGMH analysis (colored by sign(λ_2)ρ function).

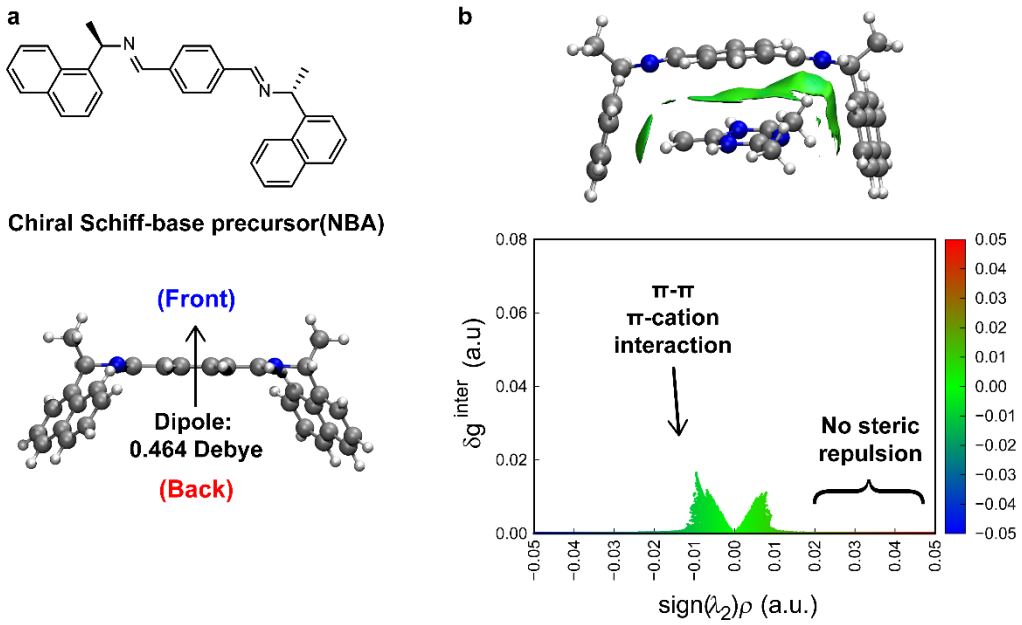

Fig. S20 (a) Structure of the chiral Schiff-base precursor with the dipole moment of 0.464 Debye, using (*R*)-(+)-1-(1-Naphthyl)ethylamine (NEA). (b) IGMH scatter map of the transitional complex (NEA). The colored real-space presentation (isovalue = 0.005) is related to the weak interaction through the IGMH analysis (colored by sign(λ_2)ρ function).

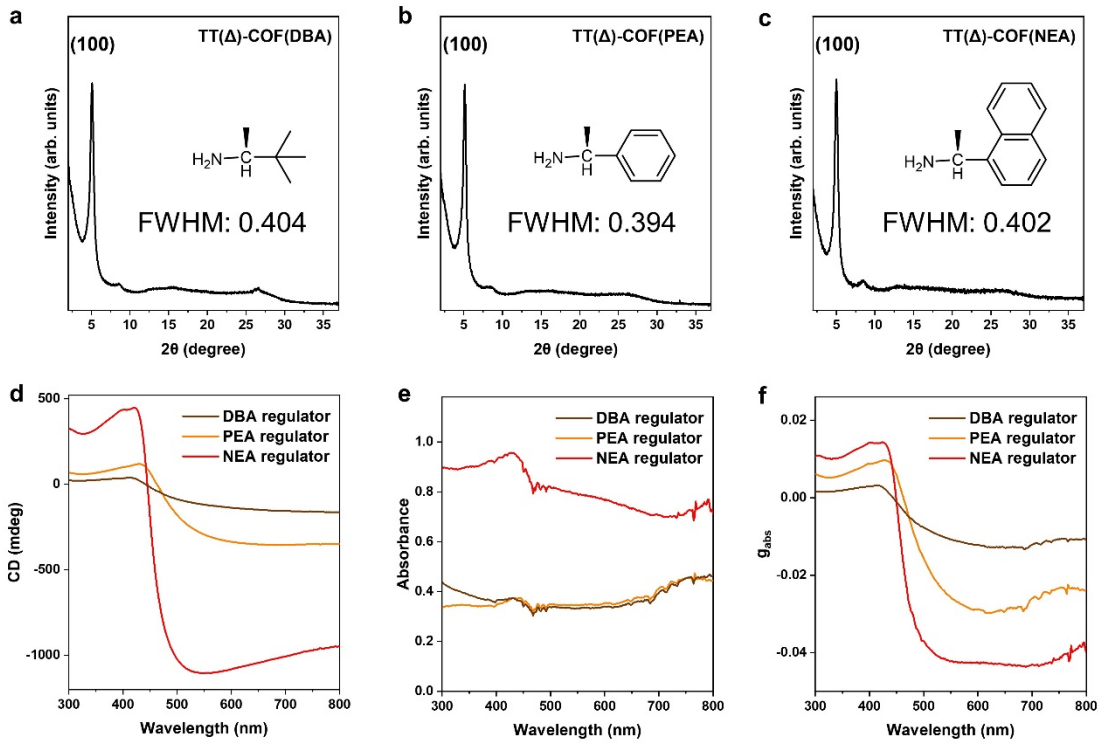

Fig. S21 (a-c) WAXS patterns of the as-synthesized TT(Δ)-COF using different chiral inducers, *i.e. S*-DBA, *R*-PEA and *R*-NEA. The FWHM of (100) peak is calculated respectively. (d) Circular dichroism spectra, (e) UV-vis spectra and (e,f) the corresponding asymmetry factor of the TT(Δ)-COF using different chiral inducers.

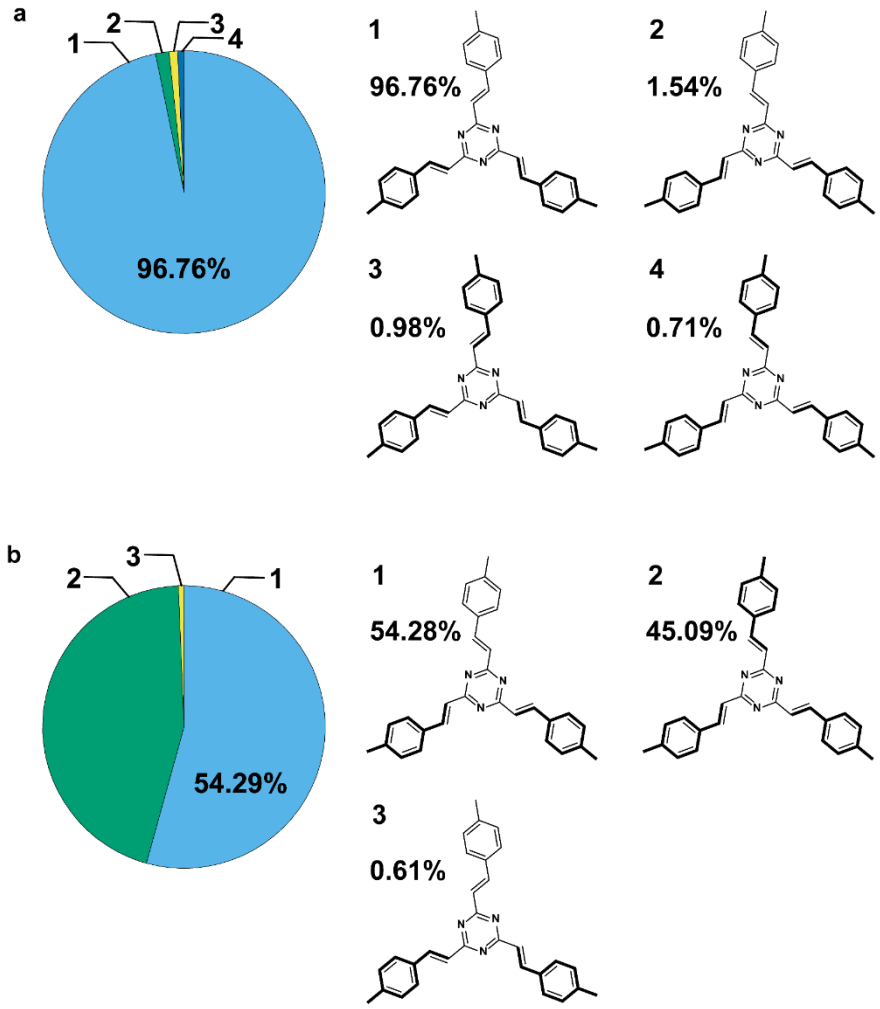

Fig. S22 Conformational Boltzmann distribution of model compound with *R*-PEA (a) and *S*-PEA (b), computed on PBE0-D3BJ/ def2-SVP level of theory.

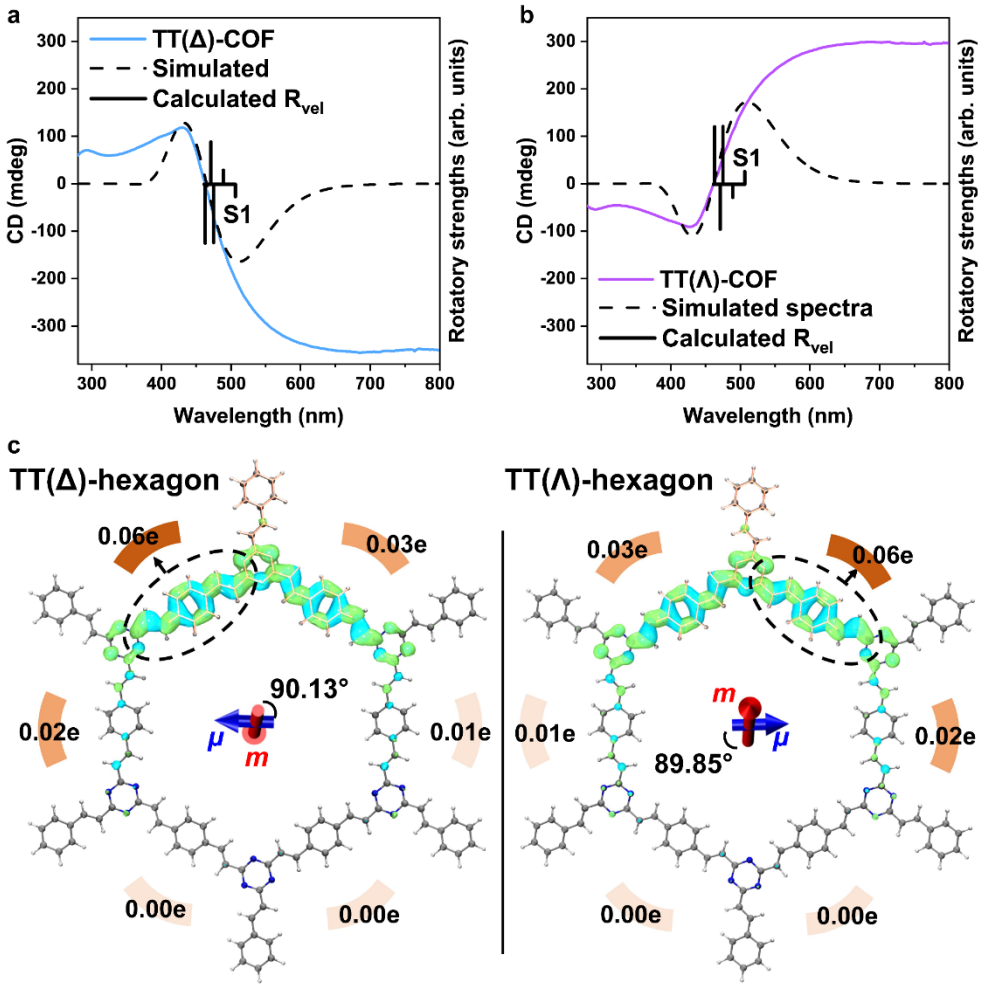

Fig. S23 (a,b) Experimentally obtained CD spectrum of TT(Δ)/(Λ)-COF (solid line), simulated CD spectrum of doubly layered TT(Δ)/(Λ)-hexagon model (dash line) and its rotatory strength of excited-state S1 to S5. (c) Photoinduced electron (green regions) and hole (blue regions) distributions of the doubly layered TT-hexagon model in the excited-state S1, wherein the top layer on the hexagon is presented with golden lines for clarity.

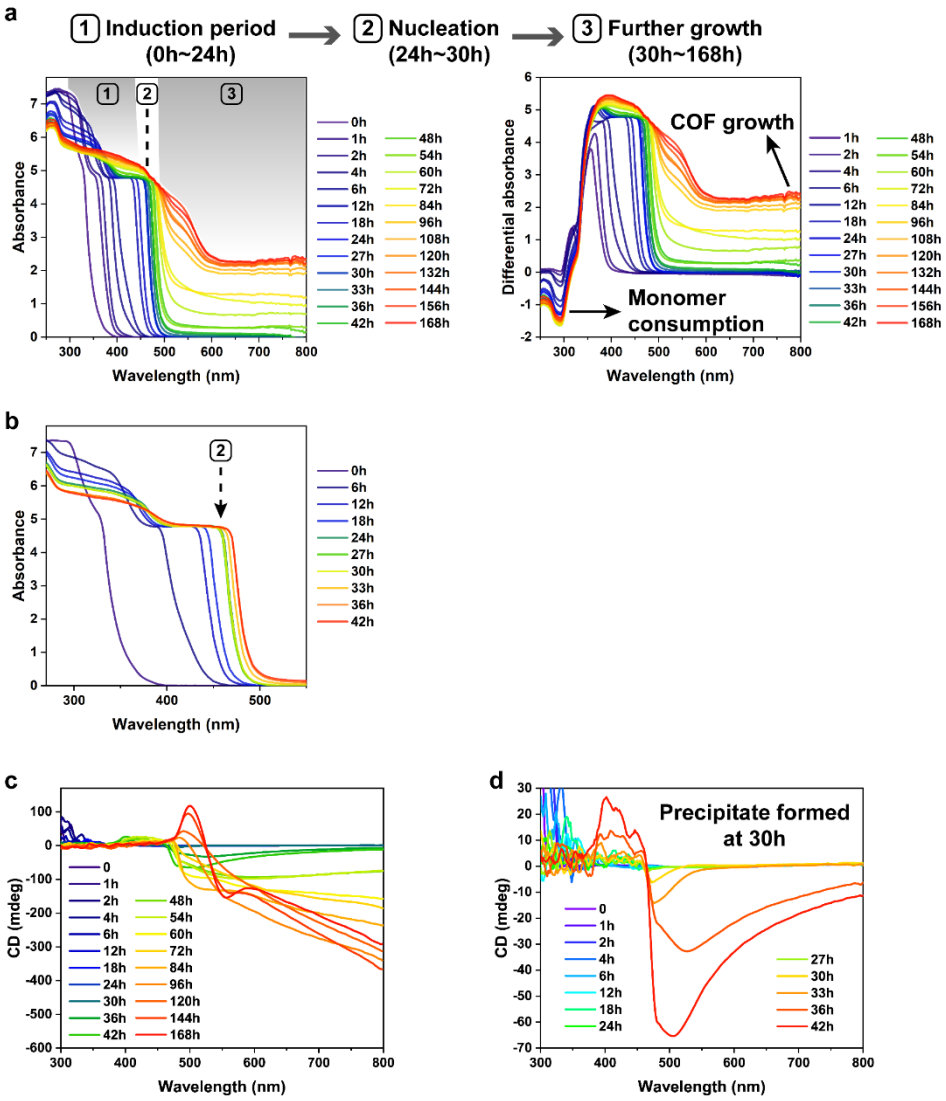

Fig. S24 (a,b) UV-vis spectra and (c,d) circular dichroism spectra for *in-situ* monitoring TT(Δ)-COF growth.

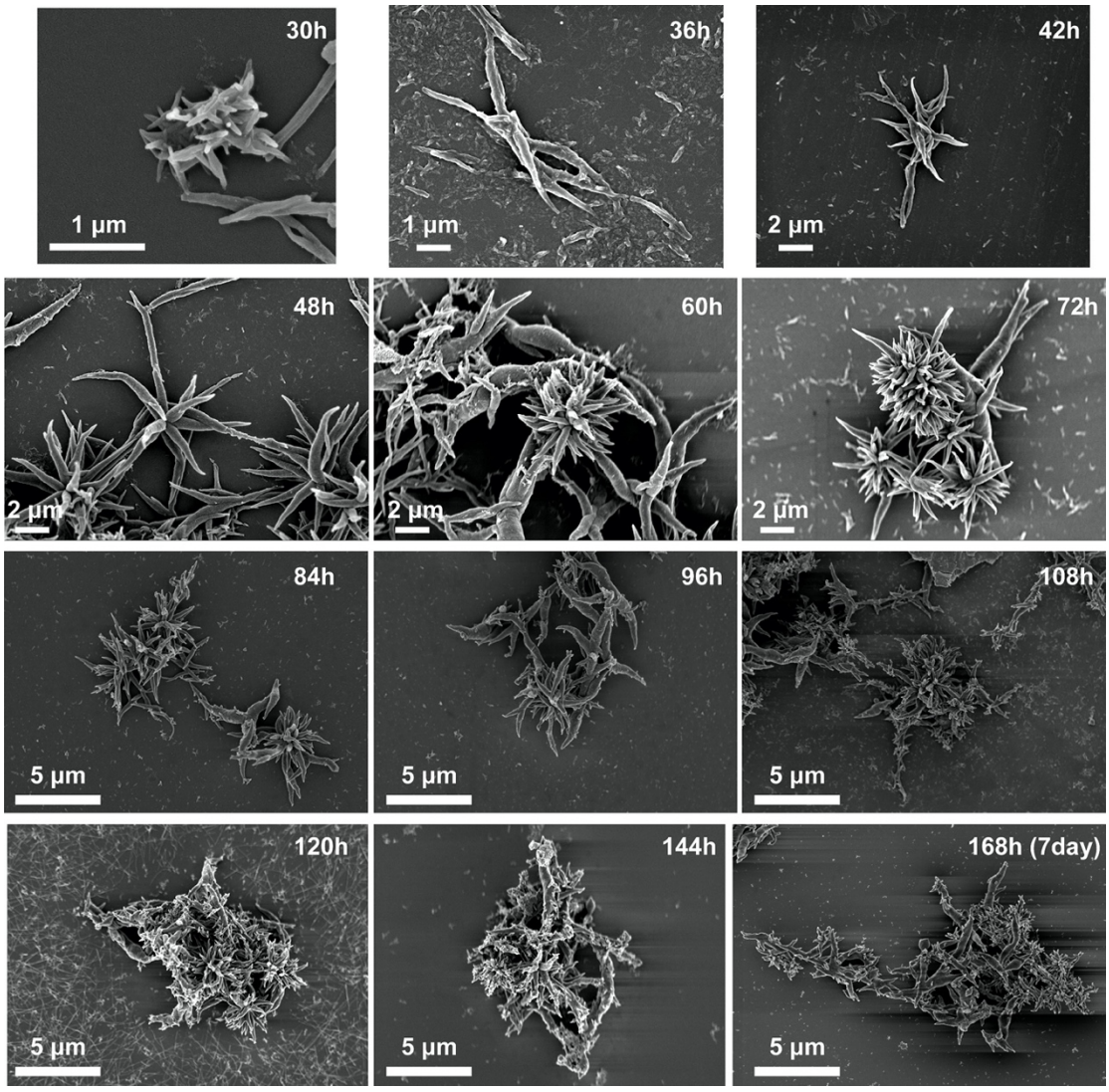

Fig. S25 SEM images for recording the evolution of TT(Δ)-COF fibers at different times.

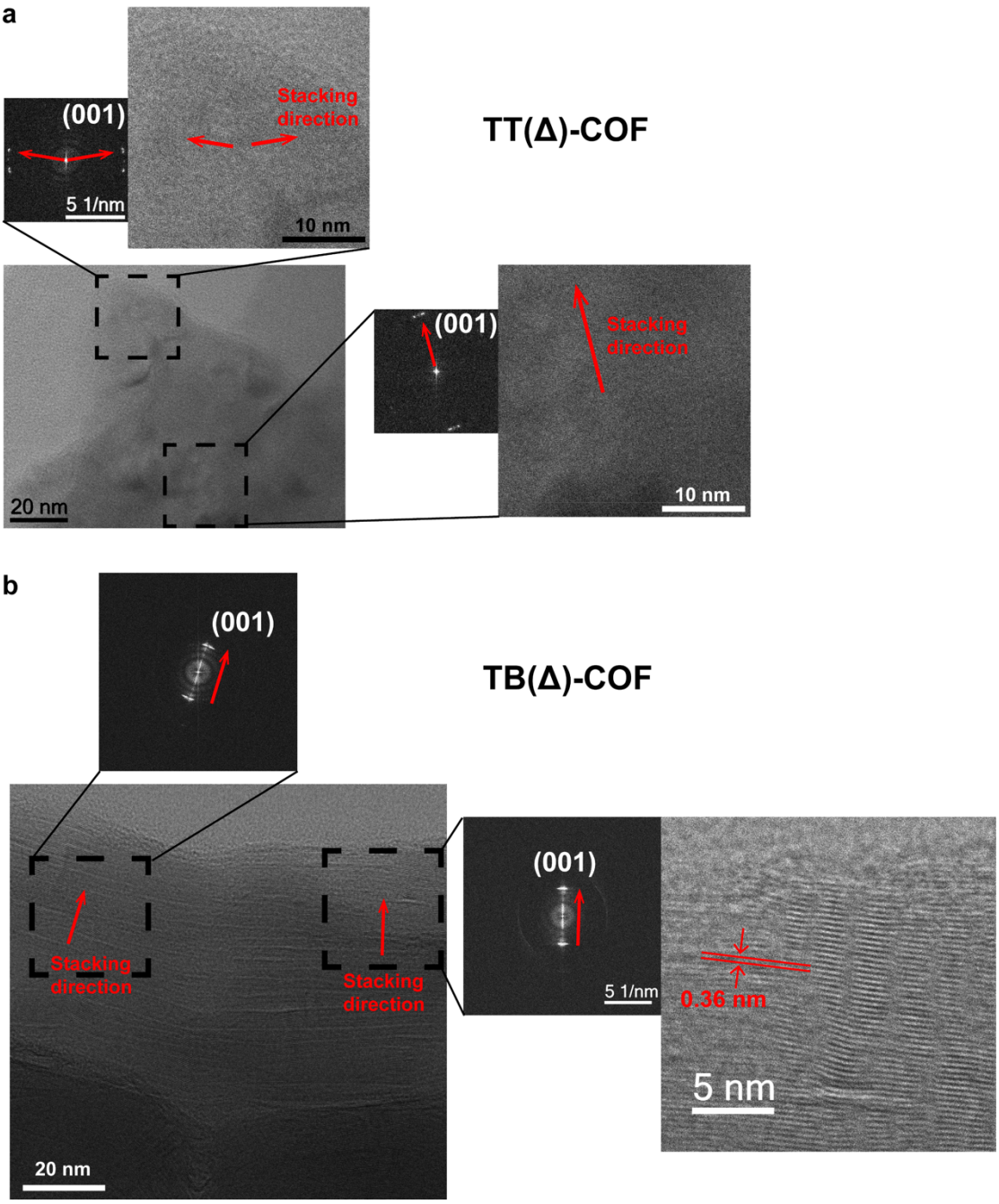

Fig. S26 HR-TEM images and FFT patterns for (a) TT(Δ)-COF fiber and (b) TB(Δ)-COF fiber.

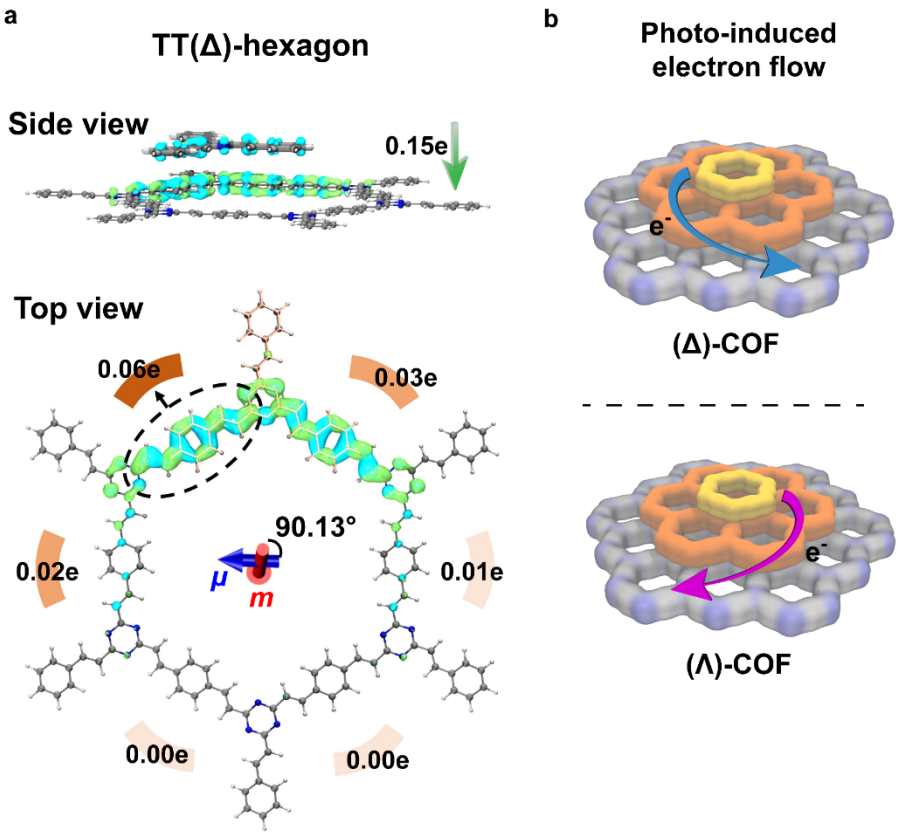

Fig. S27 (a) Photoinduced electron (green regions) and hole (blue regions) distributions of the doubly layered TT(Δ)-hexagon model in the excited-state S1, wherein the top layer on the hexagon is presented with golden lines for clarity. (b) Illustration of photoinduced electron flowing among layers along the stacked direction of chiral sp^2C-COF.

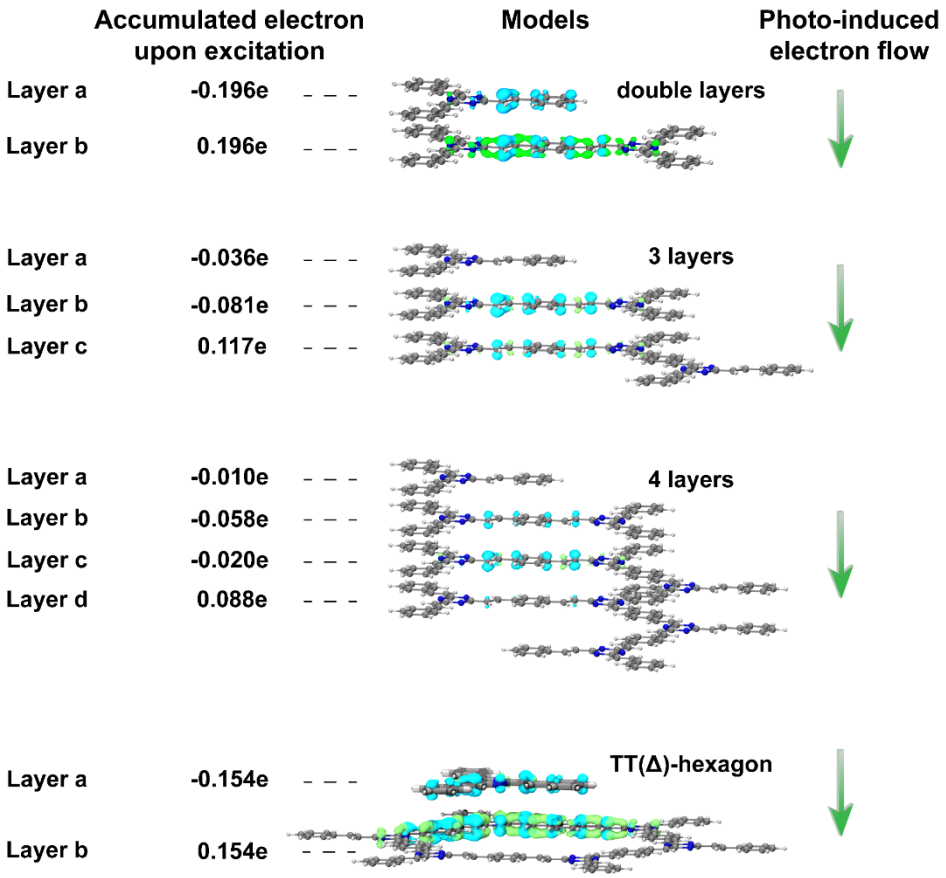

Fig. S28 The real space presentation of photoinduced electron (green regions) and hole (blue regions) distribution for the multiple layered oligomers and doubly layered TT(Δ)-hexagon in the excited state S1. The net photoelectron accumulation is shown in different layers. This calculation was computed on TD-PBE0-D3BJ/ def2-SVP level of theory.

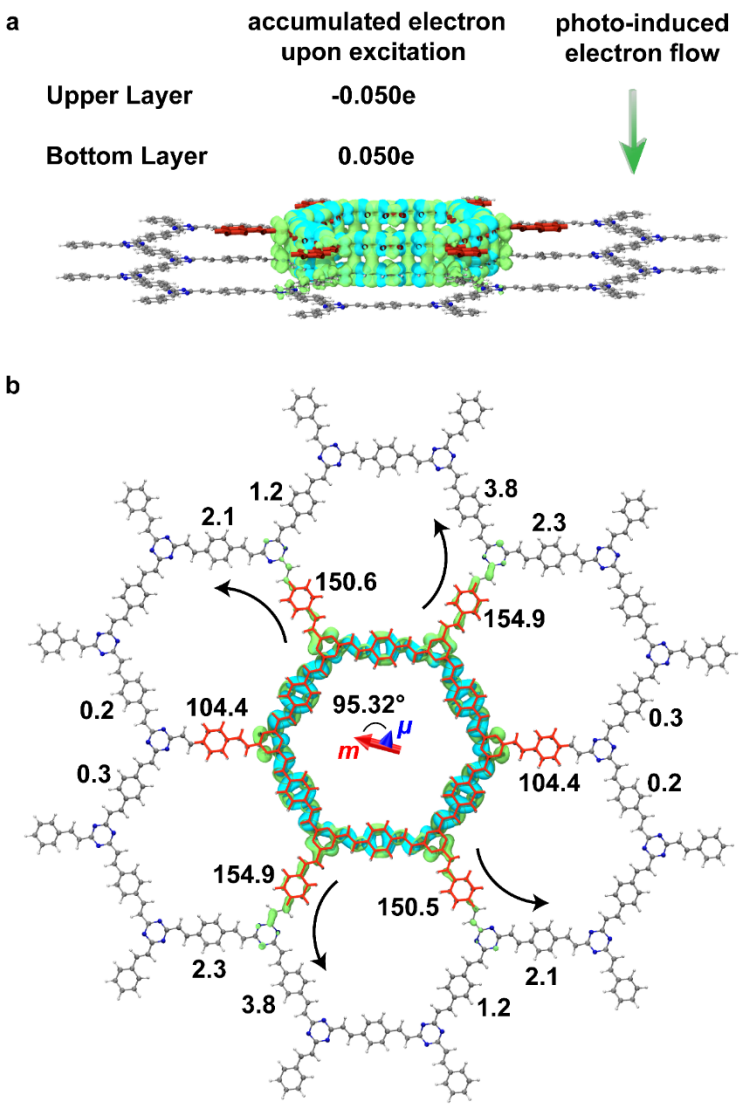

Fig. S29 (a) Side view and (b) top view of photo-induced electron (green regions) and hole (blue regions) distribution of the extended TT(Δ)-hexagonal macrocycles in the lowest excited state. In the top view, electron and hole distribution of upper layer (red skeletons) is hided, and the net accumulated photoelectrons on the branches are presented by the unit of 10^{-4} e. This study was computed on RI-ωB97X-D3/ def2-SVP level of theory, using the simplified TD-DFT (sTD-DFT) method.

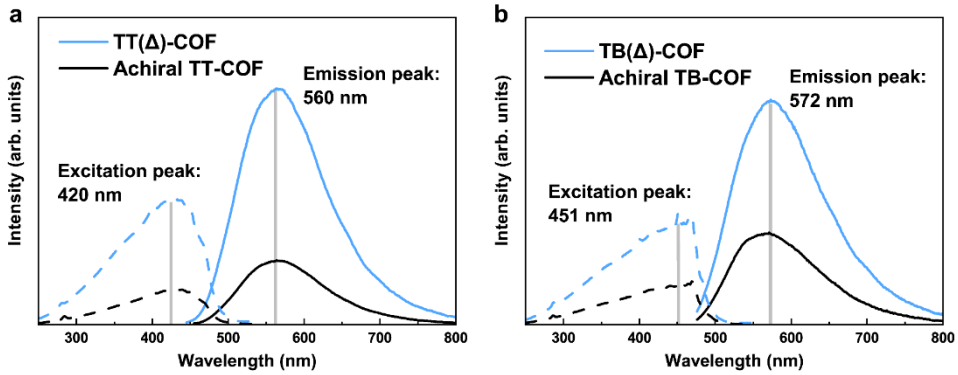

Fig. S30 Fluorescent excitation and emission spectra of (a) TT-COF and (b) TB-COF. 100mg/L samples are dispersed in ethylene glycol.

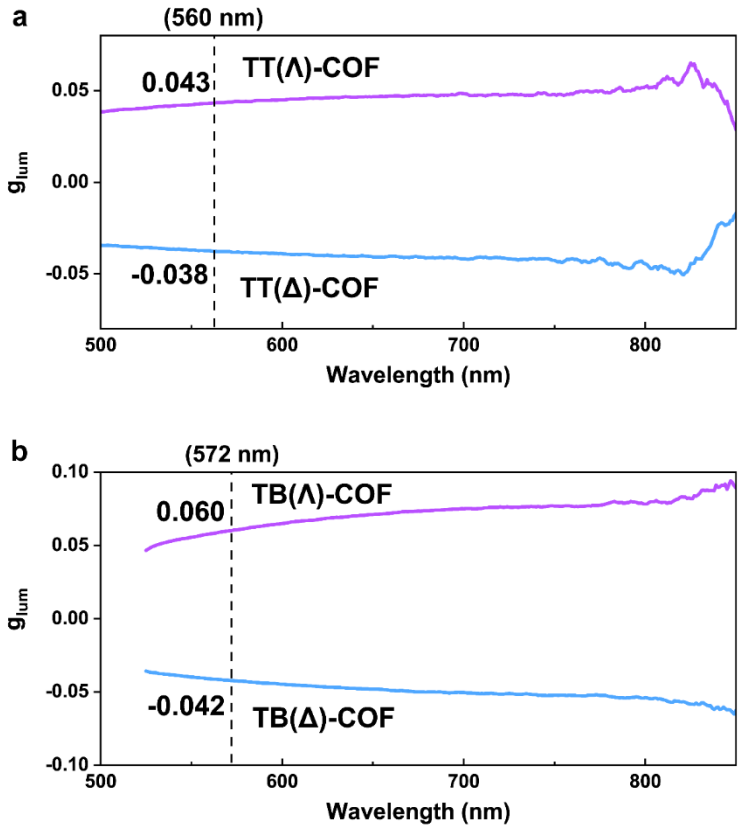

Fig. S31 Luminescence dissymmetry factors (g_{lum}) of (a) chiral TT-COF and (b) chiral TB-COF, respectively.

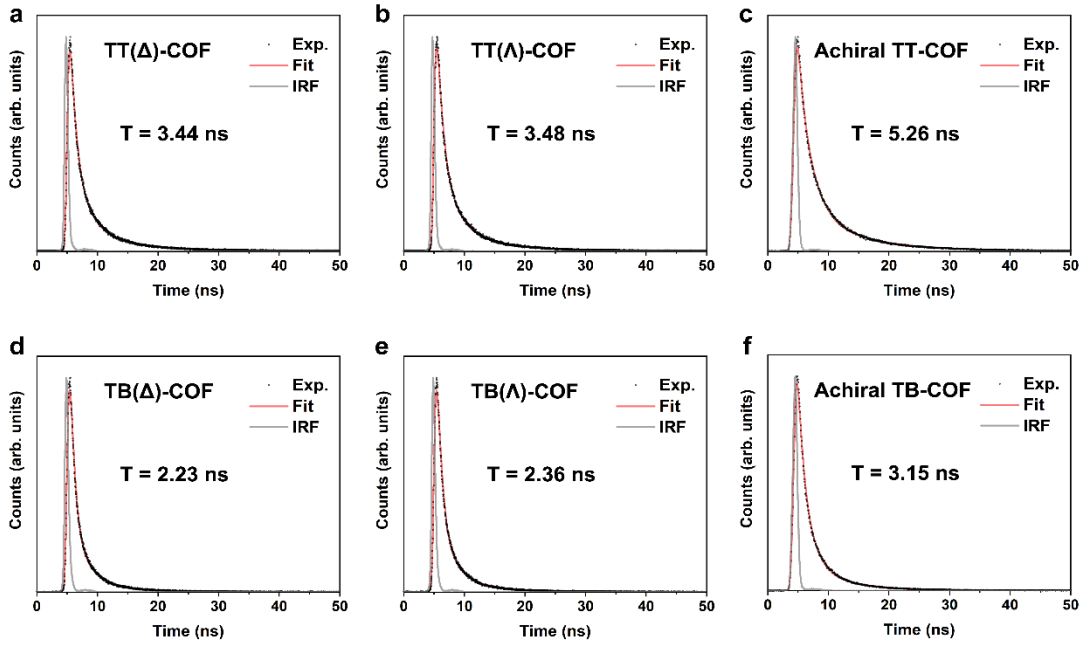

Fig. S32 Time-correlated single-photon counting measurement for (a) TT(Δ)-COF, (b) TT(Λ)-COF, (c) achiral TT-COF, (d) TB(Δ)-COF, (e) TB(Λ)-COF, and (f) achiral TB-COF, respectively. The excited wavelength is 420 nm.

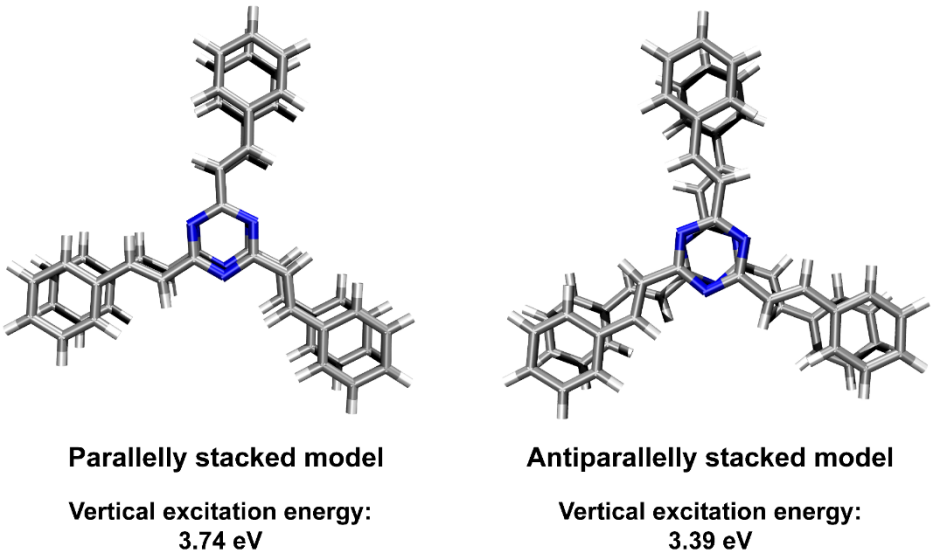

Fig. S33 Visualization of the parallelly stacked model and antiparallelly stacked model, which were cut from the corresponding periodic structures.

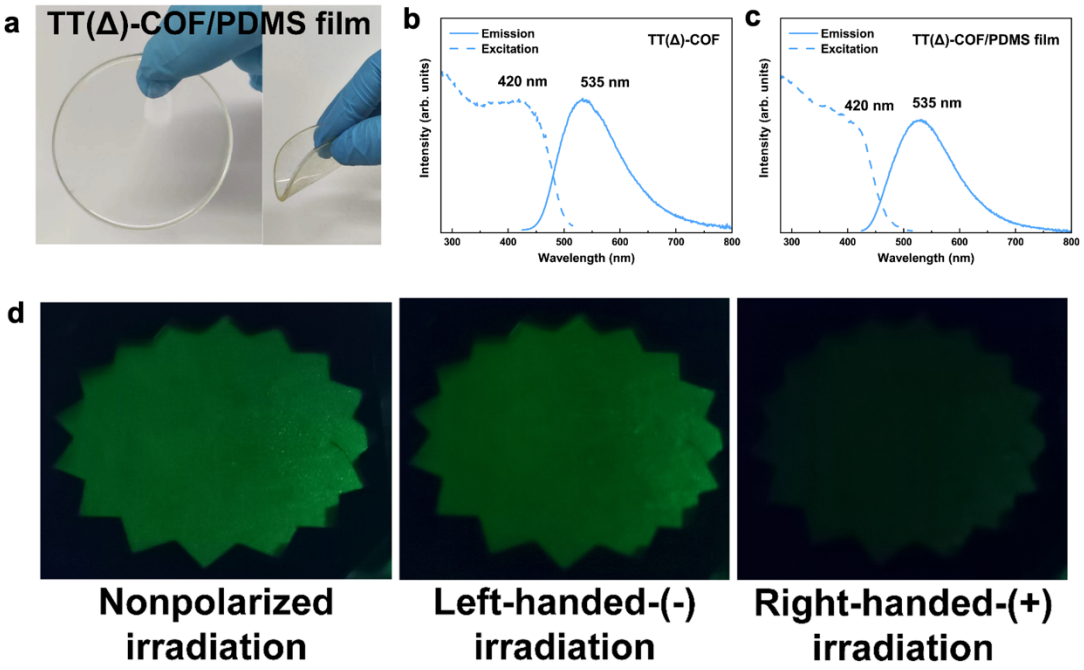

Fig. S34 (a) optical images of TT(Δ)-COF/PDMS film, (b,c) solid-state fluorescent spectra of (b) TT(Δ)-COF and (c) TT(Δ)-COF/PDMS film. (d) Fluorescence images of TT(Δ)-COF/PDMS CPL tag under the nonpolarized and polarized irradiation, respectively.

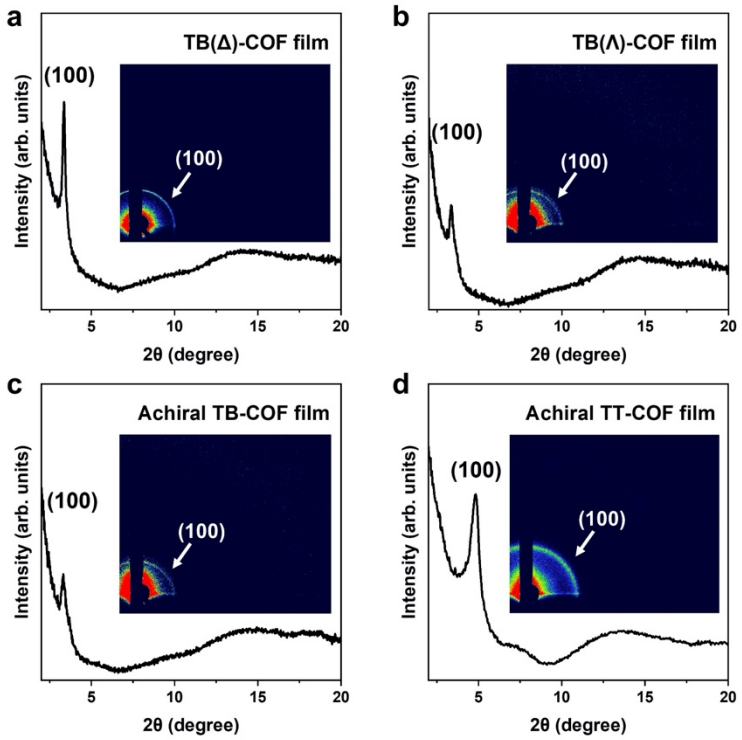

Fig. S35 GIWAXS patterns of (a) TB(Δ)-COF film, (b) TB(Λ)-COF film, (c) achiral TB-COF film and (d) achiral TT-COF film. Inset is the 2D GIWAXS patterns.

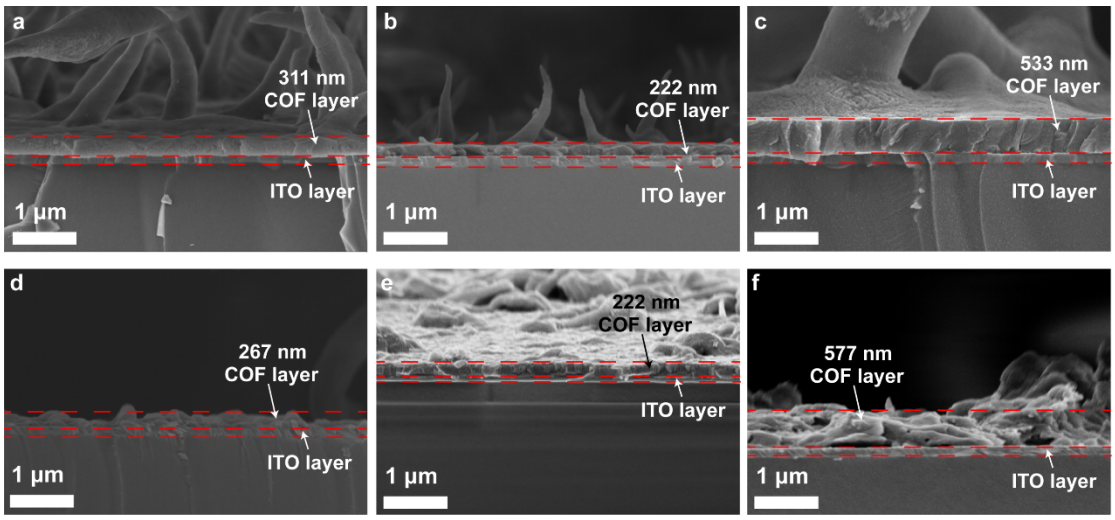

Fig. S36 The cross-sectional SEM images of (a) TT(Δ)-COF film, (b) TT(Λ)-COF film, (c) achiral TT-COF film, (d) TB(Δ)-COF film, (e) TB(Λ)-COF film and (f) achiral TB-COF film.

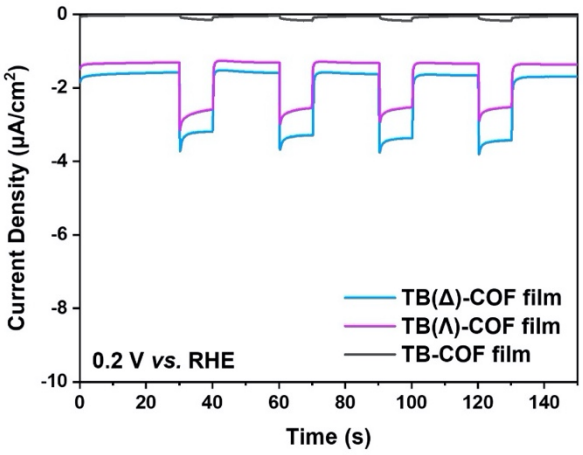

Fig. S37 The optoelectrical response of chiral and achiral TB-COF films.

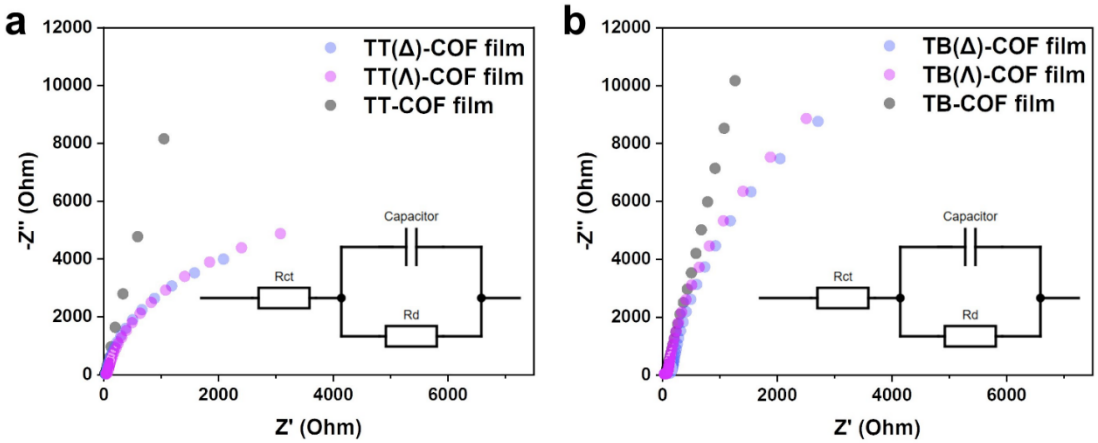

Fig. S38 EIS profiles of (a) TT-COF film and (b) TB-COF film. Inset is the equivalent circuit used for impedance analysis.

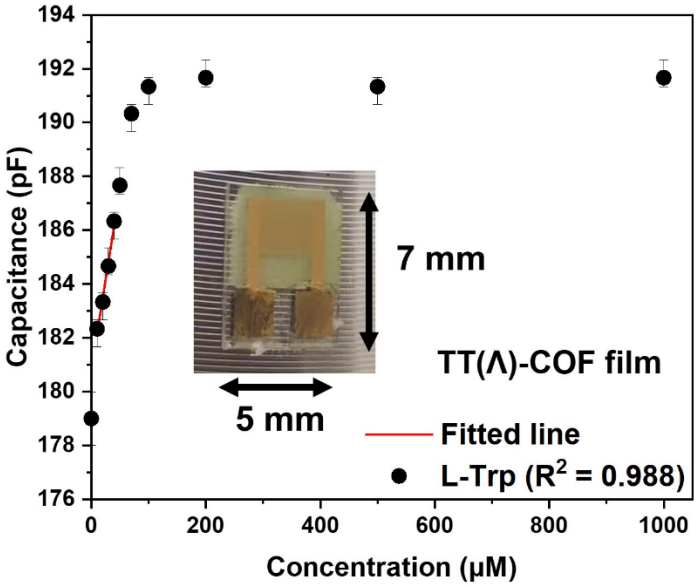

Fig. S39 Capacitance change of the TT(Λ)-COF-coated IDC sensor with increase in the concentration of L-tryptophan in ethanol.

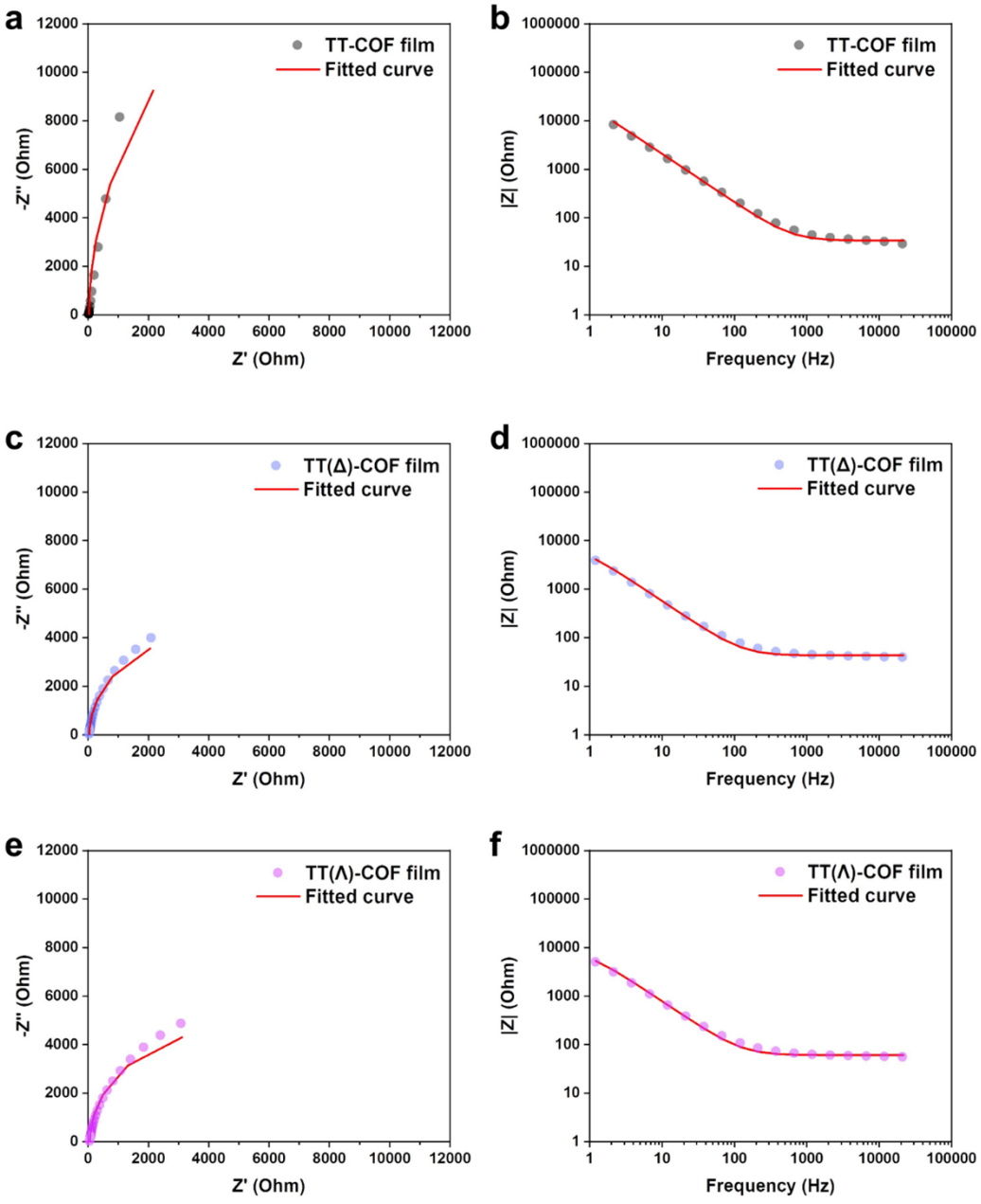

Fig. S40 Fitted Nyquist plots and impedance modulus of (a,b) TT-COF film, (c,d) TT(Δ)-COF film and (e,f) TT(Λ)-COF film.

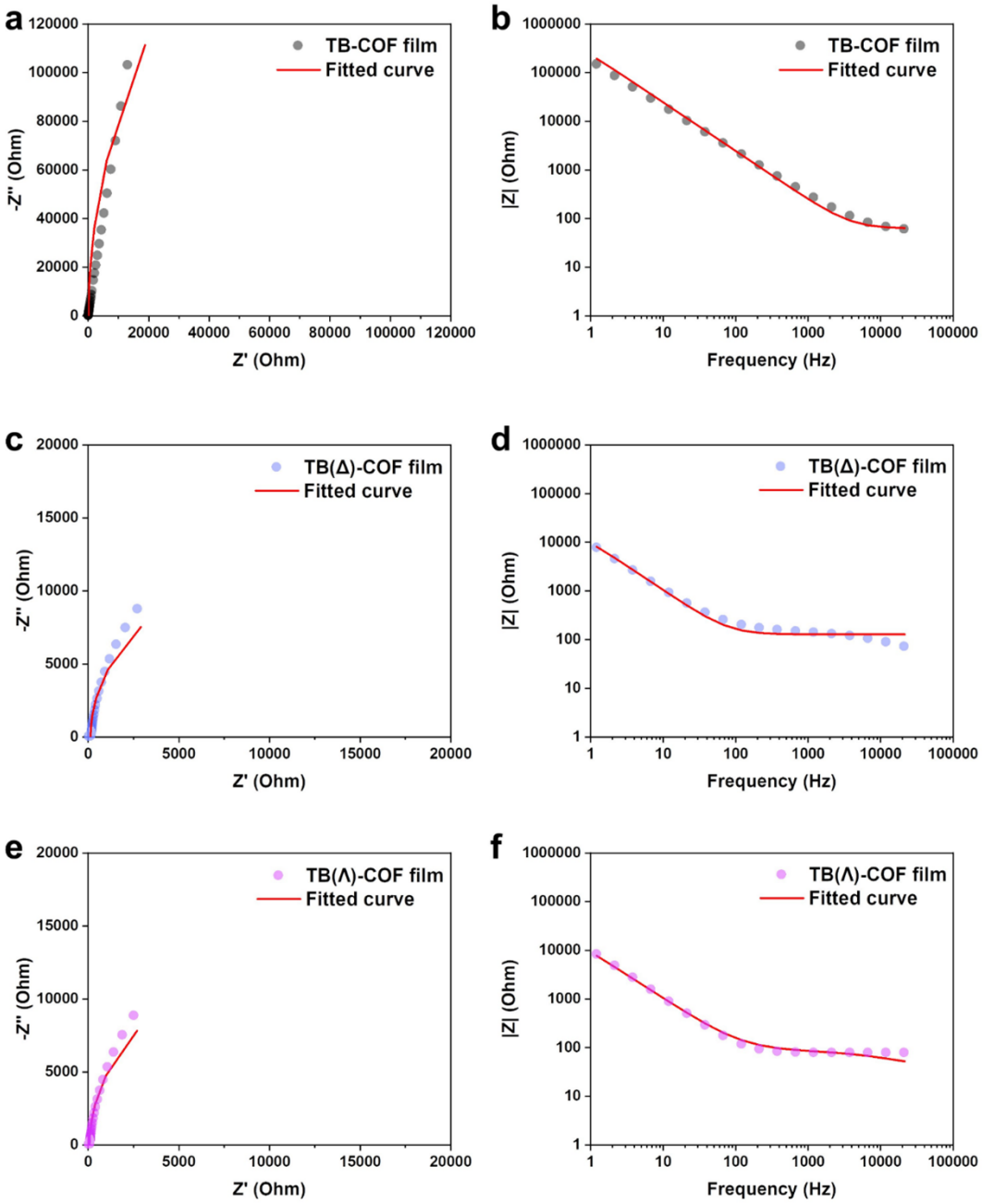

Fig. S41 Fitted Nyquist plots and impedance modulus of (a,b) TB-COF film, (c,d) TB(Δ)-COF film and (e,f) TB(Λ)-COF film.

Table S1. The FHWM and the calculated (100) domain sizes for the different chiral sp^2C-COFs.

Chiral sp^2C-COFs	**FWHM**	**(100) peak (°)**	**(100) domain (nm)**
TT(Δ)-COF	0.402	4.76	19.5
TT(Λ)-COF	0.389	4.76	20.2
Post-treated TT(Δ)-COF	0.355	4.76	22.2
TB(Δ)-COF	0.315	3.54	24.9
TB(Λ)-COF	0.297	3.54	26.4
Post-treated TB(Δ)-COF	0.256	3.54	30.7

Table S2. Conformational search of model compound with *R*-PEA, computed on PBE0-D3BJ/ def2-SVP level of theory.

Entry	**Dihedrals of -N=C-C=C- (°)**			**Free Energy (kcal/mol)**	**Ratio**
1	-0.09	-0.09	0.01	0.00	48.66%
2	-0.06	-0.03	0.03	0.18	37.18%
3	-0.17	-0.01	0.02	1.50	5.04%
4	-0.20	-0.03	0.04	1.65	4.04%
5	-0.01	-0.01	0.00	2.26	1.61%
6	0.00	0.08	0.13	2.48	1.14%
7	0.03	0.05	0.15	2.58	0.98%
8	-0.07	-0.06	-0.04	2.82	0.69%
9	-0.16	0.00	0.03	3.42	0.28%
10	-0.12	-0.05	0.18	3.95	0.12%
11	0.00	0.05	0.32	4.08	0.10%
12	-0.10	-0.04	0.21	4.24	0.08%
13	-0.32	-0.13	0.07	4.81	0.03%
14	-0.16	0.07	0.14	5.22	0.02%
15	-0.20	-0.10	-0.05	5.29	0.02%
CCDC 2344737 (Experimental)	-11.51	-8.07	11.51	/	/

Table S3. Conformational search of model compound with *S*-PEA, computed on PBE0-D3BJ/ def2-SVP level of theory.

Entry	**Dihedrals of -N=C-C=C- (°)**			**Free Energy (kcal/mol)**	**Ratio**
1	0.03	0.04	0.07	0.00	45.09%
2	-0.01	0.09	0.09	0.01	44.33%
3	-0.02	0.01	0.17	1.49	4.75%
4	-0.04	0.03	0.20	1.66	3.65%
5	-0.27	0.11	0.06	2.71	0.75%
6	-0.02	0.05	0.06	2.79	0.66%
7	-0.02	-0.01	0.16	2.97	0.51%
8	-0.01	0.03	0.13	4.16	0.08%
9	-0.11	-0.04	0.05	4.27	0.07%
10	-0.26	0.02	0.03	4.39	0.06%
11	-0.09	-0.01	0.01	4.82	0.03%
12	-0.34	-0.05	-0.05	5.68	0.01%

Table S4. Fluorescent quantum efficiency of *sp*^{2}C-COFs.

***sp*^{2}C-COFs**	**Quantum efficiency**
TT(Δ)-COF	21.9%
TT(Λ)-COF	27.5%
Achiral TT-COF	8.0%
TB(Δ)-COF	16.4%
TB(Λ)-COF	17.8%
Achiral TB(Λ)-COF	7.3%

Table S5. Comparison for the circularly polarized photoluminescence performance of organic materials in the reported literatures.

CPL materials		Luminescence dissymmetry factors $\|g_{lum}\|$	Quantum yield (%)	Figure of merit[S18]	References
COFs	**TT(Λ)-COF**	**4.3×10^{-2}**	**27.5%**	**1.2×10^{-2}**	**This work**
	TB(Λ)-COF	**6.0×10^{-2}**	**17.8%**	**1.1×10^{-2}**	
	R-COF	4.0×10^{-2}	20%	8.0×10^{-3}	[S14]
	R-TpBpy NS	2.2×10^{-2}	-	-	[S15]
	R-TpBpy/PFC/FS	9.6×10^{-2}	-	-	[S16]
	D-PDC-TZ COF@CBS	9.5×10^{-3}	-	-	[S17]
MOFs	Chiral ZIF-8	5.5×10^{-3}	40%	2.2×10^{-3}	[S18]
	L-/D-Cd-MOFs	1.2×10^{-2}	43%	5.2×10^{-3}	[S19]
	L-/D-MOFs ⊃CBS	1.2×10^{-2}	30%	3.6×10^{-3}	[S20]
	Ru-BPhen@γCD MOF	1.5×10^{-2}	16.9%	2.5×10^{-3}	[S21]
	PyC^{-}⊂CD-HF	3.5×10^{-3}	38%	1.3×10^{-3}	[S22]
MOC	$3^{R/S}$-Eu-cages	5.0×10^{-2}	2.5%	1.2×10^{-3}	[S23]
	(Eu_4L_4)(*R/S*-BINAPO)$_4$	2.0×10^{-1}	81%	1.6×10^{-1}	[S24]
	(*P*)-enantiomers	0.8×10^{-3}	-	-	[S25]
	Ir complex [2a]Cl	2.0×10^{-4}	73%	1.5×10^{-4}	[S26]
Amorphous	Nap2 liquid	5.2×10^{-2}	36.6%	1.9×10^{-2}	[S27]

organic material	(*R,S,R*)-switch 1	1.7×10^{-1}	-	-	[S28]
	p*S*-1 and p*R*-1	1.4×10^{-2}	36.6%	5.1×10^{-3}	[S29]
	(*P*)-10	1.9×10^{-3}	31%	5.9×10^{-3}	[S30]
	R/S-MIPF	4.3×10^{-3}	17.8%	7.8×10^{-3}	[S31]

Table S6. Vertical excitation energy of the parallelly stacked model, computed on TD-PBE0-D3BJ/ def2-SVP level of theory.

State	Excitation Energy (eV)	Wavelength (nm)	Oscillator Strength	MO Transition
1	3.06	406	0.00	
2	3.06	406	0.00	
3	3.12	397	0.00	
4	3.23	384	0.00	
5	3.26	381	0.00	
6	3.26	381	0.00	
7	3.58	346	0.00	
8	3.65	340	0.00	
9	3.65	338	0.00	
10	3.67	338	0.00	
11	3.70	335	0.00	
12	3.73	332	0.00	
13	3.73	332	0.00	
14	3.74	332	0.01	HOMO-10 → LUMO+1 (34.7%)
15	3.74	331	0.00	
16	3.78	328	0.02	HOMO-11 → LUMO (29.3%)
17	3.78	328	0.02	HOMO-11 → LUMO+1 (28.8%)
18	3.79	327	0.00	
19	3.80	327	0.21	HOMO-12 → LUMO+1 (34.4%)
20	3.82	326	0.21	HOMO-2 → LUMO+3 (23.9%)

Table S7. Vertical excitation energy of the antiparallelly stacked model, computed on TD-PBE0-D3BJ/ def2-SVP level of theory.

State	Excitation Energy (eV)	Wavelength (nm)	Oscillator Strength	MO Transition
1	3.38	367	0.00	
2	3.39	366	0.01	HOMO-2 → LUMO (27.2%)
3	3.39	366	0.01	HOMO-2 → LUMO+1 (27.2%)
4	3.46	358	0.00	
5	3.52	352	0.12	HOMO-2 → LUMO (48.7%)
6	3.52	352	0.12	HOMO-2 → LUMO+1 (48.9%)
7	3.56	348	0.00	
8	3.62	342	0.00	
9	3.63	342	0.14	HOMO-1 → LUMO+3 (19.3%)
10	3.63	342	0.14	HOMO → LUMO+3 (19.6%)
11	3.68	337	0.00	
12	3.68	337	0.00	
13	3.76	330	0.00	
14	3.78	328	0.25	HOMO-4 → LUMO+1 (12.4%)
15	3.78	328	0.25	HOMO-3 → LUMO+1 (12.4%)
16	3.84	323	1.63	HOMO-5 → LUMO+1 (23.7%)
17	3.84	323	1.63	HOMO-5 → LUMO (23.8%)
18	3.86	322	0.00	
19	3.88	320	0.00	
20	3.88	320	0.00	

Table S8. Impedance analysis result of *sp*^{2}C-COF films. The fitted plots are shown in **Figures S37, S38**.

***sp*^{2}C-COFs**	**Rct (Ω)**	**Rd (Ω)**	**Thickness (nm)**	**Resistivity (× 10^7 Ω·cm)**	**Fitting error**
TT(Δ)-COF	43	8300	311	27	2.2%
TT(Λ)-COF	61	9121	222	41	2.7%
Achiral TT-COF	34	42317	533	79	5.7%
TB(Δ)-COF	128	23247	267	87	7.0%
TB(Λ)-COF	78	26067	222	117	5.4%
Achiral TB-COF	63	680710	577	1180	8.5%

Table S9. Repeated sensing-regeneration cycles of capacitance *vs.* concentration (*L*-Trp) using TT(Δ)-COF-coated IDC sensors.

Entry	10 μM	20 μM	30 μM	40 μM	50 μM
1#	173.95	174.87	176.07	176.88	178.03
2#	174.49	175.51	176.59	177.37	178.19
3#	175.01	176.04	177.88	178.16	179.02
4#	174.99	175.96	177.41	177.97	178.91
5#	174.85	175.83	177.14	177.94	178.48

Table S10. Repeated sensing-regeneration cycles of capacitance *vs.* concentration (*D*-Trp) using TT(Δ)-COF-coated IDC sensors.

Entry	10 μM	20 μM	30 μM	40 μM	50 μM
1#	180.10	180.38	182.09	183.05	183.16
2#	179.82	180.02	181.89	182.95	183.02
3#	180.56	180.96	182.38	183.48	184.84
4#	180.13	180.85	182.28	183.18	183.94
5#	180.92	181.14	183.01	183.94	184.98

References

[S1] R T. Jadhav, Y. Fang, W. Patterson, C. H. Liu, E. Hamzehpoor, D. F. Perepichka, *Angew. Chem. Int. Ed.* **2019***, 58,* 13753.

[S2] T. A Betts, C. A Tipple, M. J Sepaniak, P. G Datskos, *Analytica Chimica Acta* **2000***, 422,* 89-99.

[S3] M. J. Frisch, G. W. Trucks, H. B. Schlegel, et al. *Gaussian16 Revision A.03* (Gaussian, Inc., 2016).

[S4] S. Grimme, S. Ehrlich, L. Goerigk, *J. Comput. Chem.* **2011**, *32*, 1456-1465.

[S5] J. Zheng, X. Xu, D. G. Truhlar, *Theor. Chem. Acc.* **2011**, *128*, 295–305.

[S6] C. Bannwarth, S. Grimme, *Comput. Theor. Chem.* **2014**, *1040-1041*,45-53.

[S7] F. Neese. Software update: The ORCA program system—Version 5.0. *WIREs Comput Mol Sci.* **2022**, 12:e1606.

[S8] S. Grimme, J. Antony, S. Ehrlich, H. Krieg, *J. Chem. Phys.* **2010**, *132*, 154104.

[S9] F. Neese, F. Wennmohs, A. Hansen, U. Becker, *Chemical Physics* **2009**, *356*, 98-109.

[S10] T. Lu, F. Chen. Multiwfn: A multifunctional wavefunction analyzer. *J. Comput. Chem.* **2012**, *33*, 580-592.

[S11] W. Humphrey, A. Dalke, K. Schulten. VMD: Visual molecular dynamics. *J. Mol. Graph. Model.* **1996**, *14*, 33-38.

[S12] J. Li, X. Chen, W. Zhao, Y. Guo, Y. Zhang, X. Wang, A. C.-H. Sue, X. Cao, M. Li, C. Chen, X. Wang, **2023**, *62*, e202215367.

[S13] T. D. Kühne, M. Iannuzzi, M. D. Ben, et al. *J. Chem. Phys.* **2020**, *152*, 194103.

[S14] C. Du, X. F. Zhu, C. C. Yang, M. H. Liu, *Angew. Chem. Int. Ed.* **2022**, *134*, e202113979.

[S15] H. Chen, Z. G. Gu, J. Zhang, *J. Am. Chem. Soc.* **2022**, *144*, 7245–7252.

[S16] X. Tang, X. Liao, X. Cai, J. Wu, X. Wu, Q. Zhang, Y. Yan, S. Zhang, H. Jiang, J. Fan, S. Cai, W. Zhang, Y. Liu, *Angew. Chem. Int. Ed.* **2023**, *63*, e202216310.

[S17] T. H. Zhao, J. L. Han, X. Jin, Y. Liu, M. H. Liu, P. F. Duan, *Angew. Chem. Int. Ed.* **2019**, *58*, 4978-4982.

[S18] W. L. Shang, X. F. Zhu, T. L. Liang, C. Du, L .Y. Hu, T. S. Li, M. H. Liu, *Angew. Chem. Int. Ed.* **2020**, *59*, 12811-12816.

[S19] C. Zhang, Z. P. Yan, X. Y. Dong, Z. Han, S. Li, T. Fu, Y. Y. Zhu, Y. X. Zheng, Y. Y. Niu, S. Q. Zang, *Adv. Mater.* **2020**, *32*, 2002914-2002924.

[S20] L. Hu, K. Li, W. Shang, X. Zhu, M. Liu, *Angew. Chem., Int. Ed.* **2020**, *59*, 4953– 4958.

[S21] M. Kazem-Rostami, A. Orte, M. A. Ortuño, A. H. G. David, I. Roy, D. Miguel, A. Garci, C. M. Crzu, C. L. Stern, J. M. Cuerva, J. F. Stoddart, *J. Am. Chem. Soc.* **2022**, *144*, 9380–9389.

[S22] Z. Wang, L. P. Zhou, T. H. Zhao, L. X. Cai, X. Q. Guo, P. F. Duan, Q. F. Sun, *Inorg. Chem.* **2018**, *57*, 7982-7992.

[S23] Y. Y. Zhou, H. F. Li, T. Y. Zhu, T. Gao, P. F. Yan, *J. Am. Chem. Soc.* **2019**, *141*, 19634-19643.

[S24] P. M. Burrezo, V. G. Jimenez, D. Blasi, I. Ratera, A. G. Campaña, J. Veciana, *Angew. Chem. Int. Ed.* **2019**, *58*, 16282-16288.

[S25] S. Horiuchi, T. Yamaguchi, J. Tessarolo, H. Tanaka, E. Sakuda, Y. Arikawa, E. Meggers, G. H. Clever, K. *Nat. Commun.* **2023**, *14*, 155.

[S26] X. Bai, Y. M. Sun, Y. Q. Jiang, G. J. Zhao, J. Jiang, C. H. Yuan, M. H. Liu, *Angew. Chem. Int. Ed.* **2021**, *60*, 3745-3751.

[S27] Y. R. He, S. Zhang, H. K. Bisoyi, J. H. Qiao, H. Chen, J. J. Gao, J. B. Guo, Q. Li, *Angew. Chem. Int. Ed.* **2021***, 60*, 27158-27163.

[S28] W. J. Li, Q. Y. Gu, X. Q. Wang, D. Y. Zhang, Y. T. Wang, X. He, W. Wang, H. B. Yang, *Angew. Chem. Int. Ed.* **2021**, *60*, 9507-9515.

[S29] C. Maeda, K. Nagahata, T. Shirakawa, T. Ema, *Angew. Chem. Int. Ed.* **2020**, *59*, 7813-7817 (2020).

[S30] N. Wang, R. Hong, G. Zhang, M. Pan, Y. Bao, W. Zhang, *Small* **2024**, 2409078.